Climate changes during the Lateglacial in South Europe: new insights based on pollen and brGDGTs of Lake Matese in Italy

Mary Robles[1,2], Odile Peyron[2], Guillemette Ménot[3], Elisabetta Brugiapaglia[1], Sabine Wulf[4], Oona Appelt[5], Marion Blache[2], Boris Vannière[6,7], Lucas Dugerdil[2], Bruno Paura[1], Salomé Ansanay-Alex[3], Amy Cromartie[8], Laurent Charlet[9], Stephane Guédron[9], Jacques-Louis de Beaulieu[10], Sébastien Joannin[2,4]

[1] Univ. Molise, Department of Agricultural, Environmental and Food Sciences, Campobasso, Italy
[2] Univ. Montpellier, CNRS, IRD, EPHE, UMR 5554 ISEM, Montpellier, France
[3] Univ. Lyon, ENSL, UCBL, UJM, CNRS, LGL-TPE, F-69007 Lyon, France
[4] Univ. Portsmouth, School of the Environment, Geography and Geosciences, Portsmouth, United Kingdom
[5] Helmholtz Centre Potsdam, GFZ German Research Centre of Geosciences, Section 3.6, Telegrafenberg, Potsdam, Germany
[6] Chrono-Environnement, CNRS, Univ. Bourgogne Franche-Comté, Besançon, France
[7] MSHE Ledoux, CNRS, Université Bourgogne Franche-Comté, Besançon, France
[8] Cornell Univ., Department of Anthropology, Ithaca, NY, USA
[9] Univ. Grenoble Alpes, Univ. Savoie Mont Blanc, CNRS, IRD, IFSTTAR, ISTerre, Grenoble, France
[10] Aix-Marseille Univ., CNRS, IRD, UMR 7263 & 237 IMBE, Aix-en-Provence, France

E-mails : Mary Robles, mary.robles@umontpellier.fr; Odile Peyron, odile.peyron@umontpellier.fr

Short Abstract

Quantitative climate reconstructions based on pollen and brGDGTs reveal, for the Lateglacial, a warm Bølling–Allerød and a marked cold Younger Dryas in Italy, showing no latitudinal differences in terms of temperatures across Italy. In terms of precipitation, no latitudinal differences are recorded during the Bølling–Allerød whereas the latitudes 40-42°N appear as a key junction point between wetter conditions in Southern Italy and drier conditions in Northern Italy during the Younger Dryas.

Abstract

The Lateglacial (14,700-11,700 cal BP) is a key climate period marked by rapid but contrasted changes in the Northern Hemisphere. Indeed, regional climate differences have been evidenced during the Lateglacial in Europe and the Northern Mediterranean areas. However, past climate patterns are still debated since temperature and precipitation changes are poorly investigated towards the lower European latitudes. Lake Matese in Southern Italy is a key site in the Central Mediterranean to investigate climate patterns during the Lateglacial. This study aims to reconstruct climate changes and their impacts at Matese using a multi-proxy approach including magnetic susceptibility, geochemistry (XRF core scanning), pollen data and molecular biomarkers like branched Glycerol Dialkyl Glycerol Tetraethers (brGDGTs).

Palaeotemperatures and -precipitation patterns are quantitatively inferred from pollen assemblages (multi-method approach: Modern Analogue Technique, Weighted Averaging Partial Least Squares regression, Random Forest, and Boosted Regression Trees) and brGDGTs calibrations. The results are compared to a latitudinal selection of regional climate reconstructions in Italy to better understand climate processes in Europe and in the circum-Mediterranean region. A warm Bølling–Allerød and a marked cold Younger Dryas are revealed in all climate reconstructions inferred from various proxies (chironomids, ostracods, speleothems, pollen, brGDGTs), showing no latitudinal differences in terms of temperatures across Italy. During the Bølling–Allerød, no significant changes in terms of precipitation are recorded, however, a contrasted pattern is visible during the Younger Dryas. Slightly wetter conditions are recorded south of latitude 42°N whereas dry conditions are recorded north of latitude 42°N. During the Younger Dryas, cold conditions can be attributed to the southward position of North Atlantic sea-ice and of the Polar Frontal JetStream whereas the increase of precipitation is Southern Italy seems to be linked to relocation of Atlantic storm tracks into the Mediterranean, induced by the Fennoscandian ice sheet and the North European Plain. By contrast, during the Bølling–Allerød warm conditions can be linked to the northward position of North Atlantic sea-ice and of the Polar Frontal JetStream.

Keywords: Mediterranean region; Palynology; Molecular Biomarker; Paleoclimate; Transfer functions; Tephra; Younger Dryas; Bølling–Allerød; Lateglacial

1. Introduction

In the Northern Hemisphere, the Lateglacial (ca. 14,700-11,700 cal BP) is a period of special climatic interest characterized by contrasted and rapid climate changes, associated with the successive steps of the deglaciation and changes in atmospheric and ocean circulation patterns (e.g., Walker et al., 2012; Rehfeld et al., 2018). Following the cold Oldest Dryas (OD) period, the Bølling–Allerød (B/A) or Greenland Interstadial-1 (GI-1) began abruptly at 14,700 cal BP with warmer conditions. At 12,900–11,700 cal BP, the Younger Dryas (YD) or Greenland Stadial-1 (GS-1) was the last main millennial-scale cold event in Europe during the Lateglacial (Greenland ice-core records; Rasmussen et al., 2014). The YD is characterized by extreme cold, relative dry and windy climate conditions in northern-central Europe (Hepp et al., 2019). Climate became distinctly warmer at 11,700 cal BP with the onset of the Holocene Interglacial

(Rasmussen et al., 2014). These rapid and marked climate oscillations have been observed in the Greenland ice core records (Rasmussen et al., 2014) and in Europe from various proxies such as pollen, oxygen isotopes, molecular biomarkers, beetles, and chironomids (e.g. Coope and Lemdahl, 1995; Ammann et al., 2000; Coope and Lemdahl, 1995; Peyron et al., 2005; Lotter et al., 2012; Millet et al., 2012; Blaga et al., 2013; Moreno et al., 2014; Heiri et al., 2015; Ponel et al., 2022; Duprat-Oualid et al., 2022).

Regional climate differences have been evidenced during the Lateglacial, and temperature trends in Europe and the Mediterranean region are still a matter of active research and debate. The chironomid-based synthesis of Heiri et al. (2014) suggests that temperature variations during the Lateglacial tend to be more pronounced in Western Europe (British Isles, Norway) than in Southwestern Europe, Central and Southeastern regions. This is particularly true for the Younger Dryas cooling which is not well evidenced in East and Central Southern Europe (Heiri et al., 2014). **These regional differences would be attributed to the changing position of the North Atlantic sea-ice and the Polar Frontal JetStream (Renssen and Isarin, 2001).**

Diverging temperature trends are also reconstructed from different proxies during key periods of the Lateglacial. Studies suggest that (1) the OD was cooler than the YD in Southern and Central Europe in comparison with Northern Europe (**~1-3 °C**; Heiri et al., 2014; Moreno et al., 2014); (2) the Allerød period was warmer than the Bølling in Southwestern Europe and **the** Mediterranean area (**~1°C**; Moreno et al., 2014); and (3) temperatures were more contrasted during the B/A and YD in the **Northwest** of Europe in comparison to the South of Europe (Renssen and Isarin, 2001; Moreno et al., 2014; Heiri et al., 2014). In contrast to temperature, the precipitation signal is poorly known in Europe during the Lateglacial because few proxies are available to quantitatively reconstruct precipitation change. Climate models (GCMs) simulate significant hydrological changes during the B/A and contrasted North-South patterns during the YD (Renssen and Isarin, 2001; Rea et al., 2020). They simulate drier conditions in Northern Europe and wetter conditions in Southern Europe, i.e. in the South of Italy, the Dinaric Alps, and Northern Turkey (Rea et al., 2020). Climate changes during the YD are attributed to a weak Atlantic Meridional Overturning Circulation (AMOC) and a southward shift of the Polar Frontal JetStream (PFJS), linked to the elevation of the ice sheet, in particular the Laurentide ice sheet (Renssen and Isarin, 2001; Renssen et al., 2015; Rea et al., 2020). Rea et al. (2020) also explains the regional climate patterns in Europe by a relocation of Atlantic storm tracks along the western European margin and into the Mediterranean.

The understanding of climate processes in Europe and Mediterranean regions during the Lateglacial still needs to be improved. The majority of climate reconstructions are focused on temperatures, and changes in precipitation remain elusive. The “key” junction area between Northern and Southern Europe and regional climatic patterns also needs to be better defined. Moreover, the proxies used to reconstruct climate changes (e.g., coleoptera, chironomids, pollen, ostracods, speleothems) can show differences in terms of amplitudes or patterns which are not only affected by temperatures, but also by precipitation or effective moisture (Moreno et al., 2014; Samartin et al., 2017). For these reasons, more reliable temperature reconstructions, especially from Western Europe and the Mediterranean region are required to test diverging trends during the Lateglacial. The proxies largely used to quantitatively reconstruct past climate changes are often a single proxy approach (e.g. Heiri et al., 2015; Gandouin et al., 2016; Peyron et al., 2017; Marchegiano et al., 2020; Duprat-Oualid et al., 2022). Multiproxy approaches on the same sedimentary record, including independent climate proxies, are necessary to better understand the climate processes in Europe during the Lateglacial (Lotter et al., 2012; Ponel et al., 2022). Pollen-based reconstructions have the advantage of reconstructing temperatures, precipitation, and seasonality, however, the climate signal can be perturbed by other factors such as CO_2 changes and human impact influencing vegetation development (Peyron et al., 2005). Over the last decades, novel proxies based on molecular geochemistry have been developed and molecular biomarkers are being increasingly used to reconstruct temperatures and represent a complementary proxy for lake sediments (Castañeda and Schouten, 2011). In particular, branched Glycerol Dialkyl Glycerol Tetraethers (brGDGTs) are ubiquitous organic compounds synthesized by bacteria (Weijers et al., 2006) which have been useful for **reconstructing** environmental parameters. To date, the actual producers of brGDGTs remain **elusive** although it is proposed they come from the phylum *Acidobacteria* (Weijers et al., 2009; Sinninghe Damsté et al., 2018). The relationship, however, between brGDGT distribution and environmental changes, in particular pH and temperature, are well established (Naafs et al., 2017b, 2017a; Dearing Crampton-Flood et al., 2020; Martínez-Sosa et al., 2021; Raberg et al., 2021). The degree of methylation of brGDGTs (MBT; methylation of branched GDGTs) varies depending on the mean annual air temperature (MAAT) and higher fractional abundance of hexa- (III) and penta- (II) methylated brGDGTs are recorded in colder environments (Weijers et al., 2007). Branched glycerol dialkyl glycerol tetraether (brGDGT) membrane lipids are increasingly used as a temperature proxy: in Europe, brGDGTs have been used to reconstruct the Mid to Late Holocene temperature changes in the Carpathians (Ramos-Román et al., 2022), the last 36,000 years in the Southern Iberian Peninsula (Rodrigo-Gámiz et al., 2022), the

Holocene temperatures in France (Martin et al., 2020), and in the Eastern Mediterranean over the last deglaciation (Sanchi et al., 2014; Stockhecke et al., 2021). The association in the same core between brGDGTs and other proxies such as pollen for climate reconstructions are still rare (Watson et al., 2018; **Panagiotopoulos et al., 2020**; Martin et al., 2020; Dugerdil et al., 2021a, 2021b; Ramos-Román et al., 2022; Robles et al., 2022; Rodrigo-Gámiz et al., 2022) and no studies are yet available for the circum-Mediterranean region during the Lateglacial.

This study presents a high-resolution climate reconstruction for the Lateglacial period in South Central Europe, inferred from multi-proxy data of the Lake Matese sedimentary record (Southern Italy). In detail, the aims of this study are to:

1) establish reliable and independent quantitative climate reconstructions based on molecular biomarkers (brGDGTs) and pollen data to help identify potential biases of currently used proxies and thus improve the reliability of each proxy-inferred climate record;

2) compare these reconstructions with regional climate reconstructions and in the light of other South European records;

3) better understand the climate processes in Europe and Mediterranean during the Lateglacial period.

2. Study site

Lake Matese (41°24’33.3”N, 14°24'22.1"E, 1012 m a.s.l.) is located in the Caserta province in the Campania region, Southern Italy, approximately 60 km north of the city of Naples and the active Campanian volcanoes (Vesuvius, Campi Flegrei, Ischia) (Fig. 1). The lake is situated in the Matese karst massif in the Southern Apennines, which extends over 30 km from the NE to the SW and is composed of Late Triassic-Miocene limestones and dolomites (Fiorillo and Doglioni, 2010). The present formation of the massif was the result of an extension by strike-slip faults during the Quaternary, and several strong earthquakes were recorded in the massif (Ferranti et al., 2015; Ferrarini et al., 2017; Galli et al., 2017; Valente et al., 2019). Lake Matese is the highest karst lake of Italy and is surrounded by the two highest peaks of the massif, Mount Miletto (2050 m a.s.l.) and Mount Gallinola (1923 m a.s.l.), which feed the lake by their snowmelt. Along the southern side of the lake, two sinkholes named the “Brecce” and “Scennerato” are present (Fiorillo and Pagnozzi, 2015). In the 1920s, hydraulic works were conducted to isolate the bottom of the lake and the main sinkholes by earthen dams (Fiorillo and Pagnozzi, 2015). The water level of the lake improved from 1007-1009 m a.s.l. to 1012 m a.s.l. with a volume of **15 Mm^3** (Fiorillo and Pagnozzi, 2015). A part of the lake water is transported to the hydroelectric power station of Piedimonte Matese at the bottom of the mountain massif.

The Matese Mountains are characterized by a Mediterranean warm-temperate, humid climate (Aucelli et al., 2013). The southeastern part of the massif, including Lake Matese, have the highest precipitation with a maximum **of 2167 mm** at Campitello Matese (1400 m a.s.l.) (Fiorillo and Pagnozzi, 2015). Lake Matese shows an annual precipitation of 1808 mm with a maximum in November (~290 mm) and December (~260 mm) and a minimum in July (~50 mm) (Fiorillo and Pagnozzi, 2015). The annual temperatures correspond to 9.3°C with a minimum in January (2°C) and a maximum in July (19°C) (Fiorillo and Pagnozzi, 2015).

The vegetation of the Matese massif is dominated by deciduous *Quercus* and *Ostrya carpinofolia*, while the highest altitudes at the northern flank also show an exposure of *Fagus sylvatica* and the lower altitudes of the southern flank includes Mediterranean taxa such as *Quercus ilex* (Taffetani et al., 2012; Carranza et al., 2012; Guarino et al., 2015). The hygrophilous vegetation at Lake Matese is distinguished by the presence of woody (e.g. *Salix alba, S. caprea, S. cinerea* subsp. *cinerea, Populus nigra, P. alba*), helophytes (e.g. *Phragmites australis, Schoenoplectus lacustris, Typha angustifolia, T. latifolia*) and hydrophytes species (*Myriophyllum spicatum, Persicaria amphibia*).

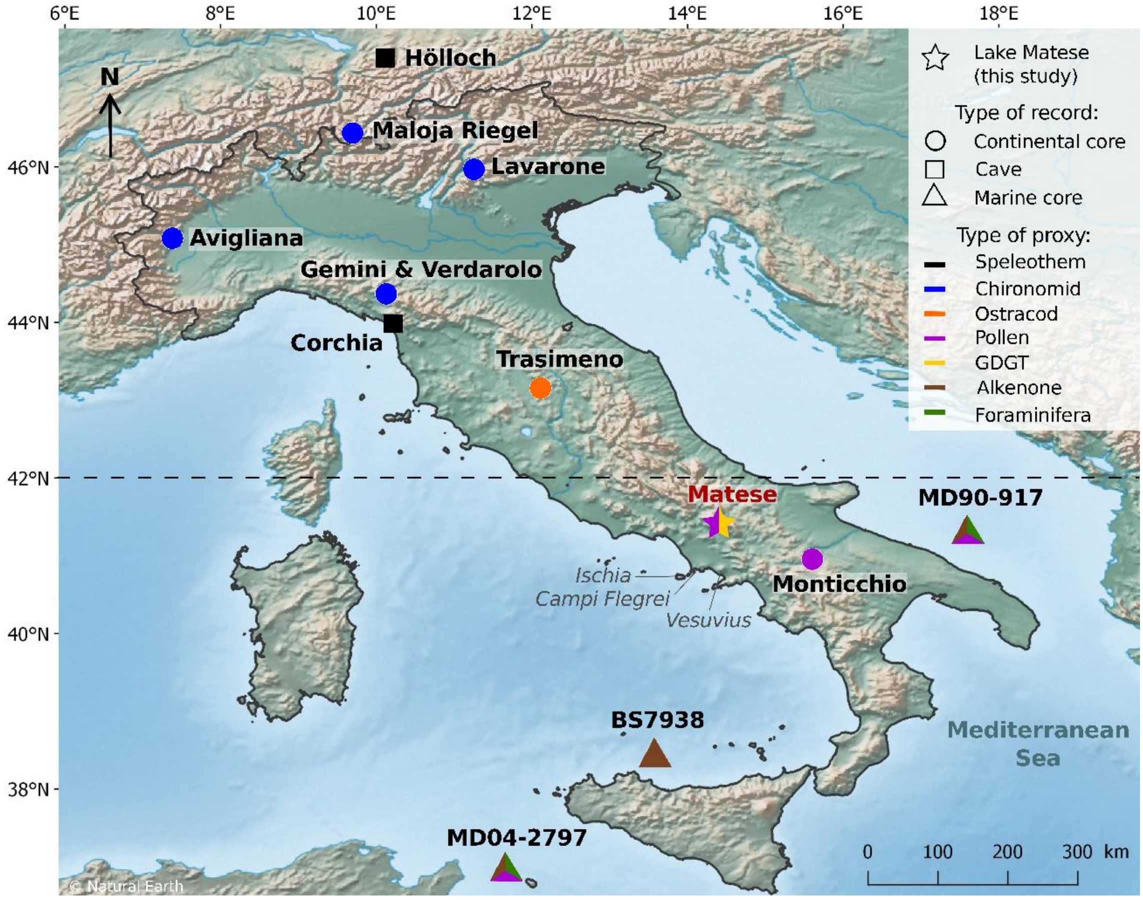

Figure 1. Location of the Lake Matese and Lateglacial paleoclimate records : Hölloch (Li et al., 2021), Maloja Riegel (Heiri et al., 2014), Lago di Lavarone (Heiri et al., 2014), Lago Piccolo di Avigliana (Larocque and Finsinger, 2008), Lago Gemini (Samartin et al., 2017), Lago Verdarolo (Samartin et al., 2017), Corchia cave (Regattieri et al., 2014), Lake Trasimeno (Marchegiano et al., 2020), Lago Grande di Monticchio (Allen et al., 2002), MD90-917 (Combourieu-Nebout et al., 2013; Sicre et al., 2013), BS7938 (Sbaffi et al., 2004), MD04-2797 (Desprat et al., 2013; Sicre et al., 2013). Dotted line indicates latitude 42°N. Location of active Campanian volcanoes (Vesuvius, Campi Flegrei, Ischia).

3. Material and methods

3.1 Coring retrieval

Coring of Lake Matese was performed in July 2019 in the southwestern part of the lake (41°24’33.3”N, 14°24'22.1"E, 1012 m a.s.l.). **Core** occurred on a floating raft composed of *Salix* spp. and *Phragmites* spp., naturally present in the eastern part of the lake. Three parallel cores (cores A, B and C) were taken with a 1 m Russian corer with a chamber diameter of 6.3 cm. The composite core, measuring 535 cm, was constructed from sections of parallel cores and is based on the lithology and XRF data.

3.2 Chronology and age-depth model

Several methods have been used to build the chronology of the core including radiocarbon dating, and tephrochronology. The regional pollen stratigraphy is used to validate this age-depth model. Twelve accelerator mass spectrometry (AMS) ^{14}C dates were measured at Poznań Radiocarbon Laboratory and at the Radiocarbon Dating Center in Lyon. Plant macrofossils (plant fibers, wood) and charcoal were selected for four samples, and bulk sediment was used for eight samples according to the sediment type. Radiocarbon ages were calibrated in years cal BP using the *Calib 8.2* software with the IntCal20 calibration curve (Reimer et al., 2020).

Visible tephra layers and cryptotephra layers, detected by magnetic susceptibility and XRF core scanning data, were subsampled and processed for geochemical analysis. Cryptotephra was extracted using H_2O_2 and HCl to remove organic matter and carbonates, sieved at 20 and 100 microns, volcanic glass shards were embedded in resin, sectioned and polished for electron probe microanalysis. A JEOL-JXA8230 probe the Helmholtz Centre Potsdam (Germany) was used with a 15kV accelerating voltage, 10 nA beam current, and a 15 micron beam size. Analytical count times were 20 seconds for all elements except for K and Na, measured first at 10 s. International glass standards such as the Max Planck Institute (MPI-glasses) ATHO-G, StHs6/80 and GOR-132 (Jochum et al., 2006) and the natural Lipari obsidian (Hunt and Hill, 1996; Kuehn et al., 2011) were measured prior to sample analysis for data quality insurance. Glass geochemical data of Matese tephras are normalized on an anhydrous, volatile-free basis and compared with published tephra glass datasets (Wulf et al., 2008; Smith et al., 2011; Tomlinson et al., 2012).

The age-depth model based on **based on one radiocarbon date and correlated tephra ages** was constructed using an interpolated linear curve with the R ‘Clam’ program with 95% confidence intervals (Blaauw, 2010). In order to validate the age depth models, the pollen stratigraphy of the regional sites was compared with pollen data of Matese. The pollen stratigraphy of Pavullo di Frignano (Vescovi et al., 2010), Lakes Accesa (Drescher-Schneider et al., 2007), Albano (Mercuri et al., 2002), Mezzano (Sadori, 2018), Monticchio (Allen et al., 2002), and Trifoglietti (De Beaulieu et al., 2017) were used to identify the OD-B/A, B/A-YD and YD-Holocene transitions. We used the median age for each transition.

3.3 Magnetic susceptibility and geochemistry

Magnetic susceptibility (MS) was measured with a MS2E1 surface scanning sensor from Bartington Instruments on a Geotek Multi-Sensor Core logger based at the Chronoenvironment laboratory (UMR CNRS - University of Franche-Comté). An interval of 3 mm or 5 mm was applied depending on the type of sediment.

Geochemical analyses were performed at high resolution by X-ray Fluorescence (XRF) with an AVAATECH core scanner at the EDYTEM laboratory (University Savoie Mont Blanc). A continuous 5 mm step measurement was applied with a run at 10 kV and 0.1 mA for 15 s to detect lightweight elements, such as Al, Si, K, Ca, Ti, Mn, Fe and a second run at 30 kV and 0.15 mA for 20 s to detect Br, Rb, Sr and Zr. The XRF core scanning provides an estimate of the geochemical composition, and the results are semi-quantitative and expressed as peak intensities counts i.e. counts per second (cps).

3.4 Pollen analyses

A total of 56 samples from the Matese core were collected at 4 cm or 6 cm resolution for pollen analysis. For each sample, 1 cm^3 of sediment was processed and 3 *Lycopodium* tablets were added to estimate pollen concentration. Samples were treated following the standard procedure (Faegri et al., 1989; Moore et al., 1991) including HCl, KOH, sieving, acetolysis and HF. The pollen **concentrates** were analyzed with a Leica DM1000 LED microscope at a standard magnification of 400x. Pollen taxa were identified using photo atlases (Beug, 2004; Reille, 1998; Van Geel, 2002) and a modern reference collection (ISEM, University of Montpellier). Each slide was counted with a minimum of 300 terrestrial pollen grains, excluding aquatic plants such as Cyperaceae, aquatic taxa, and fern spores. A simplified pollen diagram was constructed **(Fig. 2)** with the R package *Rioja* (Juggins and Juggins, 2020). **This study presents the main pollen taxa and is not focused on variations of individual species.**

3.5 Pollen-inferred climate reconstruction

A multi-method approach was used to reconstruct climate parameters from pollen data with **greater** reliability than reconstructions based on a single climate reconstruction method (Peyron et al., 2013, 2011, 2005; Salonen et al., 2019). We have selected here the Modern Analog Technique (MAT; Guiot, 1990), Weighted Averaging Partial Least Squares regression (WAPLS; ter Braak and van Dam, 1989; ter Braak and Juggins, 1993), and the most recent machine-learning methods : Random Forest (RF; Breiman, 2001; Prasad et al., 2006) and Boosted Regression Trees (BRT; De'ath, 2007; Elith et al., 2008).

The MAT is an assemblage approach, based on the measure of the degree of dissimilarity (squared chord distance) between fossil and modern pollen assemblages (Guiot, 1990). Fossil pollen assemblages are compared to a set of modern assemblages (modern dataset), each one associated with climate estimates. The closest modern samples are retained and averaged to estimate past climate conditions (annual and seasonal temperature and precipitation). WAPLS is a non-linear regression technique that models the relationships between the climate parameters and the pollen taxa from a modern pollen dataset, before applying these relationships to fossil pollen assemblages (ter Braak and Juggins, 1993; ter Braak and van Dam, 1989). WAPLS and MAT methods are applied with the R package *Rioja* (Juggins and Juggins, 2020). RF and BRT, based on machine learning, utilizes regression trees developed with ecological data, and has been used recently to reconstruct palaeoclimatic changes (Salonen et al., 2019; Robles et al., 2022). These classification trees are used to partition the data by separating the pollen assemblages based on the relative pollen percentages. RF is based on a large number of regression trees, each tree being estimated from a randomized ensemble of different subsets of the modern pollen dataset by **bootstrapping** (Breiman, 2001; Prasad et al., 2006). Finally, the RF prediction is applied **to** the fossil pollen record. BRT is also based on regression trees (De'ath, 2007; Elith et al., 2008); it differs from RF in the definition of the random modern datasets. In RF, each sample gets the same probability of being selected, while in BRT the samples that were insufficiently described in the previous tree get a higher probability of being selected. This approach is called 'boosting' and increases the performance of the model over the elements that are least well predicted (Breiman, 2001; Prasad et al., 2006; De'ath, 2007; Elith et al., 2008). RF is applied with the R package *randomForest* (Liaw and Wiener, 2002) and BRT with the R package *dismo* (Hijmans et al., 2021).

The modern pollen dataset (n = 3373 sites) used for the calibration of the methods is based on the large Eurasian/Mediterranean dataset compiled by Peyron et al. (2013, 2017) and completed by Dugerdil et al. (2021a) and Robles et al. (2022). In our study, we added pollen data of 92 surface lake sediments from Italy (Finsinger et al., 2007) and 15 moss polsters from the Matese massif (Robles, 2022). Then, a biome constraint (Guiot et al., 1993), based on the pollen-Plant Functional Type method and following the biomization procedure (Peyron et al., 1998; Prentice et al., 1996) was applied to modern and fossil pollen samples. The modern pollen dataset finally selected for the calibration of the different methods contains 1018 samples belonging to 3 biomes depicted in the fossil core: "warm mixed forest" (WAMX), "temperate deciduous" (TEDE) and "cold steppe" (COST). Performance of each method and calibration training was statistically tested (for more details, see Dugerdil et al., 2021a) to determining if modern samples are suitable for quantitative climate reconstructions. The Root Mean Square Error (RMSE) and the R^2 are presented in the Supplementary Table S1. Five climate parameters were reconstructed, mean annual air temperature (MAAT), mean temperature of the warmest month (MTWA), mean temperature of the coldest month (MTCO), mean annual precipitation (PANN), and winter precipitation (P_{winter} = December, January, and February). For each climate parameter, the methods fitting with the higher R^2 and the lower RMSE were selected. Cyperaceae and ferns in the Matese record have been excluded because they are associated with local dynamics.

3.6 BrGDGT analyses

A total of 56 samples from the Matese core (4 cm or 6 cm resolution) were used for GDGT analysis (same as for pollen analysis). The samples were freeze-dried, powdered and subsampled (1 g for clay and 0.4 g for gyttja). Lipids were extracted from the sediment using a microwave oven (MARS 6; CEM) with dichloromethane:methanol (3:1). Then, the internal standard was added (C_{46} GDGT, Huguet et al., 2006). The total lipid extracts were separated into apolar and polar fractions using a silica SPE cartridge with hexane:DCM (1:1) and DCM:MeOH (1:1). The polar fractions containing brGDGTs were analyzed using a High-Performance Liquid Chromatography Mass Spectrometry (HPLC-APCI-MS, Agilent 1200) with detection via selective ion monitoring (SIM) of m/z 1050, 1048, 1046, 1036, 1034, 1032, 1022, 1020, and 1018 in the LGL-TPE of ENS Lyon (Hopmans et al., 2016; Davtian et al., 2018). GDGT concentrations were calculated based on the internal standard **(C_{46} GDGT, Huguet et al., 2006).** The analytic reproducibility was assessed **by regularly processing a lab-internal sediment sample (Vaux Marsh; 45°57’21.1”N, 5°35’32.42”E). Analytical precision is based on duplicate injections of one sample of each Matese core lithological types (n=4). Respective analytical 1-sigma standard deviations are then applied to each measurement within one lithology.**

3.7 GDGTs annual temperature reconstruction

The proportion of tetra- (I), penta- (II) and hexa- (III) methylated brGDGTs includes the fractional abundances of the 5-methyl (X), 6-methyl (X’) and 7-methyl (X7) brGDGTs (Ding et al., 2016). The CBT **(cyclization ratio of branched tetraethers)** and MBT indexes were defined by Weijers et al. (2007) and the MBT'_{5me}, only based on the 5-methyl brGDGTs, by De Jonge et al. (2014). The Mean Annual Air Temperature (MAAT) was reconstructed with global (Sun et al., 2011) and East African (Russell et al., 2018) lacustrine calibrations. The mean temperature of Months Above Freezing (MAF) was reconstructed with a lacustrine calibration based on Bayesian statistics (Martínez-Sosa et al., 2021; *https://github.com/jesstierney/BayMBT*) and a global lacustrine calibrations with revised compound fractional abundances based on methylation and cyclization number and methylation position (Raberg et al., 2021). Synthesis of the formulae for the main brGDGT indices are presented in Table 1. Modern MAAT and MAF of the Lake Matese corresponds to 9.3 °C.

The analytic reproducibility corresponds to ±0.040 for CBT, ±0.0167 for MBT, ±0.0206 for MBT'$_{5me}$, ±0.8566 °C for MAAT developed by Sun et al. (2011), ±0.6672 °C for MAAT developed by Russell et al. (2018), and ±0.5403 °C and ±1.1258 °C for MAF$_{Meth}$ and MAF$_{Full}$ developed by Raberg et al. (2021).

Table 1. Synthesis of the formulae for the main brGDGT indices. For acronym explanation of MAF$_{Meth}$ and MAF$_{Full}$, see Raberg et al. (2021). For more information about the Bayesian statistics see Martínez-Sosa et al., 2021 and references therein.

Indice	Formula	Reference
$\%tetra$	$\frac{Ia + Ib + Ic}{\Sigma brGDGTs}$	Ding et al., 2016
$\%penta$	$\frac{IIa + IIa' + IIa_7 + IIb + IIb' + IIb_7 + IIc + IIc' + IIc_7}{\Sigma brGDGTs}$	Ding et al., 2016
$\%hexa$	$\frac{IIIa + IIIa' + IIIa_7 + IIIb + IIIb' + IIIb_7 + IIIc + IIIc' + III}{\Sigma brGDGTs}$	Ding et al., 2016
CBT	$-log\frac{Ib + IIb}{Ia + IIa}$	Weijers et al., 2007
MBT	$\frac{Ia + Ib + Ic}{\Sigma brGDGTs}$	Weijers et al., 2007
MBT'_{5me}	$\frac{Ia + Ib + Ic}{Ia + Ib + Ic + IIa + IIb + IIc + IIIa}$	De Jonge et al., 2014
$MAAT\ (°C)$	$3.949 - 5.593 \times CBT\ + 38.213 \times MBT$ $(n = 100, R^2 = 0.73, RMSE = 4.27°C)$	Sun et al., 2011
$MAAT\ (°C)$	$-1{,}21 + 32.42 \times MBT'_{5me}$ $(n = 65, R^2 = 0.92, RMSE = 2.44\ °C)$	Russell et al., 2018
$MAF_{Meth}(°C)$	$92.9 + 63.84 \times fIb^2_{Meth} - 130.51 \times fIb_{Meth}$ $- 28.77 \times fIIa^2_{Meth} - 72.28 \times fIIb^2_{Meth}$ $- 5.88 \times fIIc^2_{Meth} + 20.89 \times fIIIa^2_{Meth}$ $- 40.54 \times fIIIa_{Meth} - 80.47 \times fIIIb_{Meth}$ $(n = 182, R^2 = 0.90, RMSE = 2.14\ °C)$	Raberg et al., 2021
$MAF_{Full}(°C)$	$-8.06 + 37.52 \times fIa_{Full} - 266.83 \times fIb^2_{Full}$ $+ 133.42 \times fIb_{Full} + 100.85 \times fIIa'^2_{Full}$ $+ 58.15 \times fIIIa'^2_{Full} + 12.79 \times fIIIa_{Full}$	Raberg et al., 2021

	$(n = 182, R^2 = 0.91, RMSE = 1.97\ °C)$	
$MAF\ (°C)$	$Equation\ from\ the\ Bayesian\ model:$ $MBT'_{5me} = 0.030(\pm 0.001)MAF + 0.075(\pm 0.012)$ $(R^2 = 0.82, RMSE = 2.9\ °C)$	Martínez-Sosa et al., 2021

4. Results

4.1 Lithology, magnetic susceptibility, **XRF** and pollen

The lithology of **the** Matese core (Fig. 2) is mainly composed of gray clay sediment with vivianite from the base to 350 cm, interrupted by an organic layer between 477-484 cm (sedimentary Unit 2) and a **macroscopically** visible tephra layer (Fig. 2) between 476-437 cm (sedimentary Unit 3). This part contains few plant fibers, which are essentially vertically oriented in the core. From 349 to 320 cm, the lithology is formed by a mix of clay sediment and gyttja (sedimentary Unit 5). This part is mostly composed by roots and **fine rootlets.**

Magnetic susceptibility (MS) and Potassium (K) peaks of XRF core scanning are used to detect tephra layers (Fig. 2). MS and Potassium contents show increased values at 516-502 cm, 482-437 cm and 366-338 cm, which correspond to the deposition of tephra material (macroscopic visible tephra and cryptotephra of primary and secondary deposition). Small peaks are also visible in MS between 430 and 360 cm but they are not associated with any observed tephra. Potassium content is also marked by an increase between 536-526 cm which corresponds to tephra of primary deposition. Titanium (Ti) content, on the other hand, is representative for terrigenous input which is prevailing in sedimentary Unit 4 (Fig. 2).

The main pollen taxa diagram (Fig. 2) shows the dominance of herbaceous taxa (Poaceae, *Artemisia*) and a small proportion of arboreal taxa at the base of the sequence. From 520 to 425 cm, the period is marked by three expansion phases of arboreal taxa, followed between 438 to 354 cm by a large increase of *Artemisia* and a drop of AP taxa starting at 422 cm. Finally, from 354 to 338 cm AP and Poaceae increase, whereas *Artemisia* significantly decline.

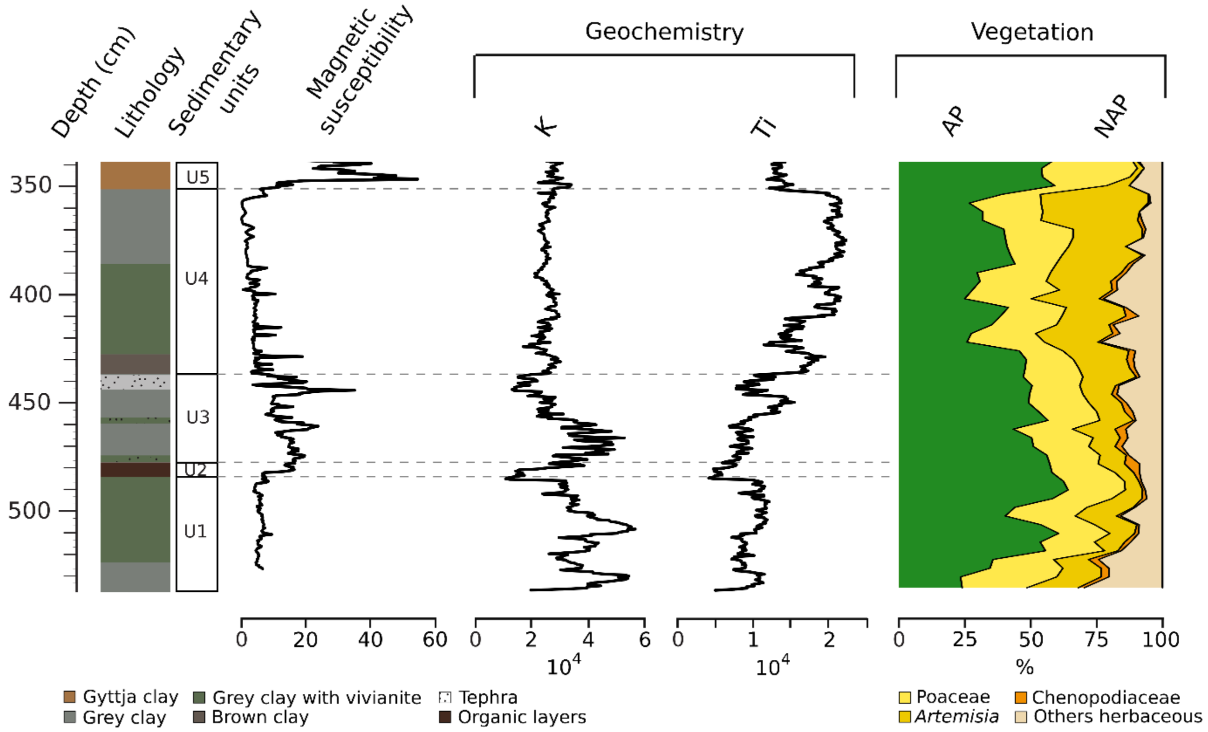

Figure 2. Sediment lithology, magnetic susceptibility, geochemical data and selected terrestrial pollen taxa of Matese. Arboreal Pollen (AP; green) and Non Arboreal Pollen (NAP; yellow-orange) are expressed in percentages of total terrestrial pollen.

4.2 Age-depth model

The age-depth model is based on ^{14}C dates and tephrochronology, and then pollen stratigraphy was used to validate the age-depth model (Fig. 3). Based on their typical phono-trachytic and bimodal tephri-phonolitic to trachytic major element glass composition Matese tephras at 530 cm and 346 cm depth can be correlated with distal Monticchio tephras TM-8 and TM-6-2, respectively (Fig. 4; Table 2). Tephra TM-8 has been correlated with the Neapolitan Yellow Tuff (NYT) eruption (Wulf et al., 2004) which has an age of 14,194 ± 172 cal BP (Bronk Ramsey et al., 2015). The tephra layer at 530 cm corresponds to the primary deposition and secondary deposition of remobilised tephras that were identified at 510 cm and 475 cm. TM-6-2 most likely are derived from the Early Holocene Casale eruption from Campi Flegrei (Smith et al., 2011) which is varve dated in Monticchio at 11,210 ± 224 cal BP (Wulf et al., 2008). The tephra layer at 346 cm corresponds to a primary deposition.

The ages obtained with the regional pollen stratigraphy show an OD-B/A transition at 14,500 ± 93.7 cal BP, a B/A-YD transition at 12,800 ± 57.7 cal BP and a YD-Holocene transition at 11,575 ± 103.1 cal BP (Allen et al., 2002; Mercuri et al., 2002; Drescher-Schneider et al., 2007; Vescovi et al., 2010; De Beaulieu et al., 2017; Sadori, 2018). Pollen stratigraphy of the regional sites were compared with pollen data of Matese and the ages obtained show a good correspondence with the ages of tephra samples but a poor correspondence with the ^{14}C dates. Therefore, most of the ^{14}C dates (Table 3) are not included in the age-depth model (except the date at the base of the core). **The organic matter extracted from sediment was essentially composed of rootlets, that explains the rejuvenation of the ^{14}C ages.**

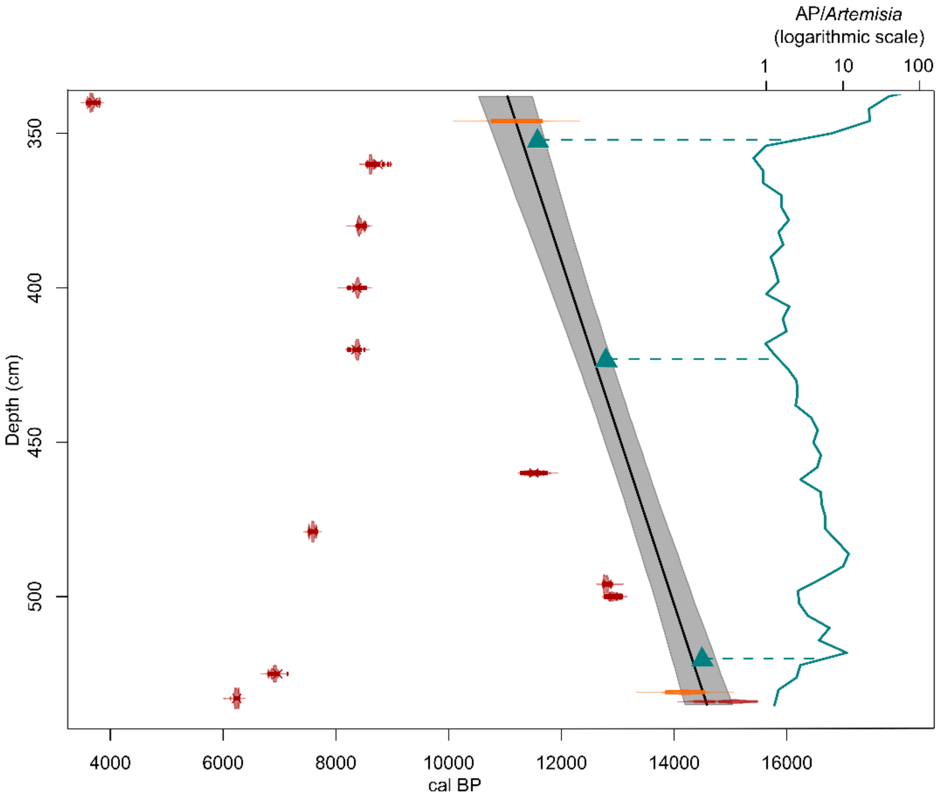

Figure 3. Age-depth model is based on calibrated AMS radiocarbon dates (red points; Table 3) and tephra ages (orange points; Table 2). **The grey band is the 95% confidence interval**. Blue triangles are the median of ages of the vegetation transition compiled with the regional pollen stratigraphy. This pollen stratigraphy includes the sites of Pavullo di Frignano (Vescovi et al., 2010), Accesa (Drescher-Schneider et al., 2007), Albano (Mercuri et al., 2002), Mezzano (Sadori, 2018), Monticchio (Allen et al., 2002), and Trifoglietti (De Beaulieu et al., 2017). AP/Artemisia ratio (blue line) is expressed on a logarithmic scale. AP: Arboreal Pollen.

Table 2. Tephra samples from Matese cores (MC) and correlation with tephra samples from Lago Grande di Monticchio (Wulf et al., 2008) and proximal eruptive sources.

Sample ID	Depth MC (cm)	Tephra Monticchio	Eruption	Age (cal BP)	Age reference
C1 96-97	346	TM-6-2	Casale	11,210 ± 224	Wulf et al., 2008
A5 75-77	475 (reworked)	TM-8	Neapolitan Yellow Tuff (NYT)	14,194 ± 172	Bronk Ramsey et al., 2015
C3 83-84	510 (reworked)				
B5 95-96	530				

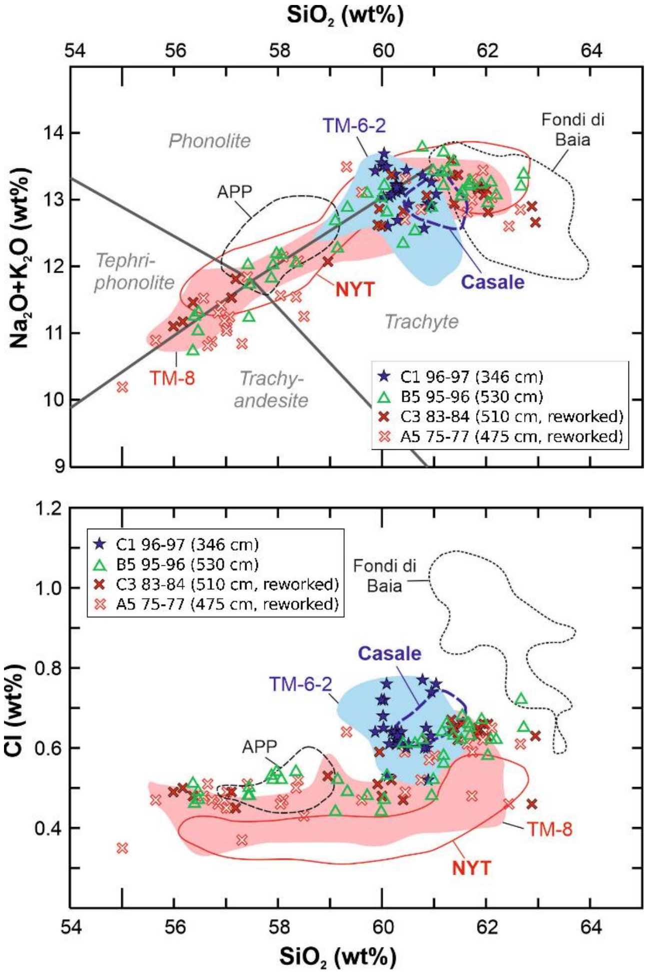

Figure 4. Bivariate plot of selected major elements (SiO_2 vs. total alkalis and SiO_2 vs. Cl) of Matese tephras and potential proximal and Monticchio tephra correlatives. Data from: TM-6-2 (Monticchio, Wulf et al., 2008; this study); TM-8 (Monticchio, Tomlinson et al., 2012; this study); Casale, Fondi di Baia (proximal; Smith et al., 2011); APP/Agnano Pomici Principali and NYT/Neapolitan Yellow Tuff (proximal; Tomlinson et al., 2012).

Table 3. AMS-radiocarbon dates (Radiocarbon Laboratory, Poznań), calibrated median ages, with 2 σ range of calibration from Matese cores (MC).

Sample ID	Depth MC (cm)	Lab code	Material	AMS ^{14}C age (BP)	Age (cal BP) (2 σ)	Median age (cal BP)
A4 40-41	340	Poz-128971	Bulk	3425 ± 30	3573 - 3822	3668
A4 60-61	360	Poz-138111	Bulk	7850 ± 40	8540 - 8968	8631
A4 80-81	380	Poz-138112	Bulk	7640 ± 50	8370 - 8541	8432
B4 50-51	400	Poz-128972	Bulk	7580 ± 60	8206 - 8519	8385
A5 20-21	420	Poz-138113	Bulk	7570 ± 50	8206 - 8512	8379
A5 60-61	460	Poz-128976	Bulk	10020 ± 50	11280 - 11743	11519
A6 52-53	479	Poz-119283	Plant fibers, wood fragments, charcoals	6730 ± 40	7513 - 7669	7596
A5 96-97	496	Poz-137155	Wood fragments	10870 ± 60	12728 - 12903	12799
B5 64-65	500	Poz-128973	Bulk	11000 ± 60	12769 - 13078	12925
A6 98-99	525	Poz-119284	Plant fibers	6060 ± 35	6795 - 7147	6912
B5 97-98	533	60747	Plant fibers	5430 ± 30	6190 - 6295	6236
B5 98-99	534	Poz-128975	Bulk	12650 ± 130	14331 - 15477	15027

4.3 Pollen-inferred climate reconstructions

Pollen-inferred climate reconstructions at Matese show similar trends for all methods (Fig. 5). The MAT and the BRT methods show higher sample-to-sample variability than the WAPLS, and RF appears as the less sensitive method. Statistical results of the model performance (Supplementary Table S1) show the better values for R^2 and RMSE for the BRT method (all climatic parameters).

Temperature trends show two cold periods (phases 1 and 3) and two warm periods (phases 2 and 4). The reconstructed values (MAAT and MTWA) during the warm periods are close to modern values whereas the values of MTCO are lower than the modern values. Annual precipitation (PANN) shows few variations and the values of PANN and P_{winter} are lower than modern values, with all methods. Phase 1 (535-530 cm; 14,600-14,500 cal BP) is characterized by cold conditions and low precipitation during winter. Phase 2 (530-436 cm; 14,500-12,800 cal BP) is a warm period characterized by strong warming and punctuated by three colder events at 14,000 cal BP, 13,500-13,350 cal BP and 13,000 cal BP. Mean annual precipitation shows little variation whereas P_{winter} shows higher values than during the phase 1. Phase 3 (436-367 cm; 12,800-11,570 cal BP) is a strong event marked by cold conditions, a slight decline in P_{winter} and few changes for PANN. At the transition with phase 4, a significant decrease in the precipitation parameters is recorded. Phase 4 (367-338 cm; 11,570-11,000 cal BP) is characterized by a well-marked temperature increase (MAAT and MTCO) associated with wet conditions (hydrological parameters reach their maximum value).

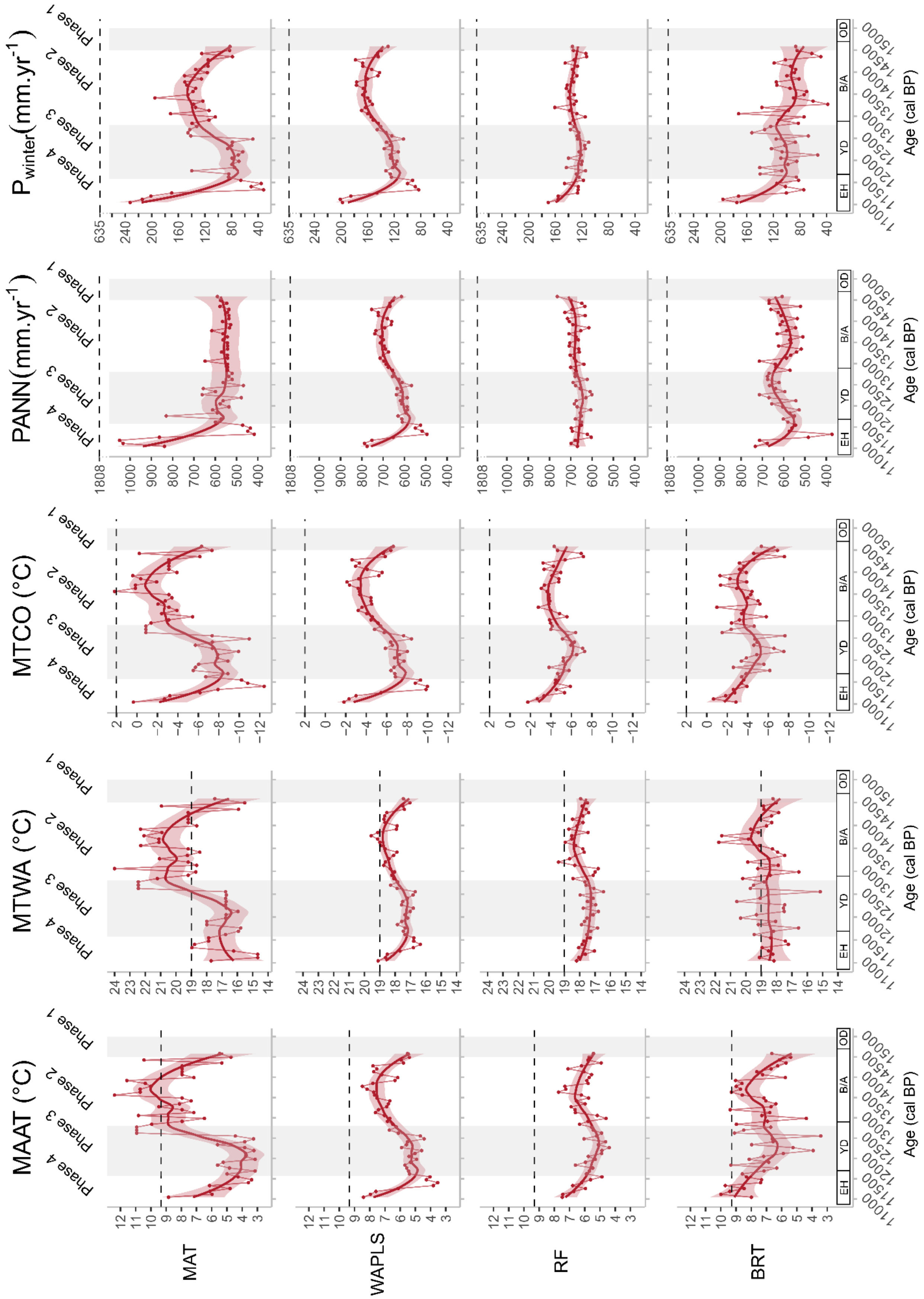
MAAT (°C)
MTWA (°C)
MTCO (°C)
PANN(mm.yr^{-1})
P$_{winter}$(mm.yr^{-1})
MAT
WAPLS
RF
BRT
Phase 4
Phase 3
Phase 2
Phase 1
EH
YD
B/A
OD
Age (cal BP)
11000
11500
12000
12500
13000
13500
14000
14500
15000
12
11
10
9
8
7
6
5
4
3
24
23
22
21
20
19
18
17
16
15
14
2
0
−2
−4
−6
−8
−10
−12
1808
1000
900
800
700
600
500
400
635
240
200
160
120
80
40

Figure 5. Lake Matese pollen-inferred climate reconstruction based on four methods against age: MAT (Modern Analogue Technique), WAPLS (Weighted Averaging Partial Least Squares regression), RF (Random Forest) and BRT (Boosted Regression Trees). Large lines correspond to loess smoothed curves, shaded areas to the 95% confidence interval and **dashed** lines to modern climate values of Lake Matese. MAAT: mean annual air temperature. MTWA: mean temperature of the warmest month. MTCO: mean temperature of the coldest month. PANN: mean annual precipitation. P_{winter}: winter precipitation. **OD: Oldest Dryas. B/A: Bølling–Allerød. YD: Younger Dryas. EH: Early Holocene.**

4.3 BrGDGT-inferred climate reconstruction

4.3.1 Concentration and distribution of brGDGTs

The total concentration of brGDGTs ranges between 0.06 and 8.63 $\mu g.g^{-1}$ dry sediment. The fractional abundances of brGDGTs (Fig. 6A) show a dominance of pentamethylated brGDGTs (II, 46%), especially brGDGT IIa (23%), brGDGTs IIa' (7%) and brGDGTs IIb (6%). The relative abundance of tetramethylated brGDGTs (I, 33%) is mainly explained by brGDGT Ia (20%) and brGDGTs Ib (9%). The relative abundance of hexamethylated brGDGTs (III, 21%) is mainly explained by brGDGT IIIa (11%) and brGDGTs IIIa' (6%). The relative abundances of tetra, penta- and hexamethylated brGDGTs of Matese core are compared to global datasets (Fig. 6B). Sediment samples of the Matese core show a good correspondence with global lake and soil samples, except for some samples from sedimentary Unit 1 and 5. Samples of sedimentary Unit 5, characterized by a mix of clay and gyttja, are more similar to global soil and peat samples.

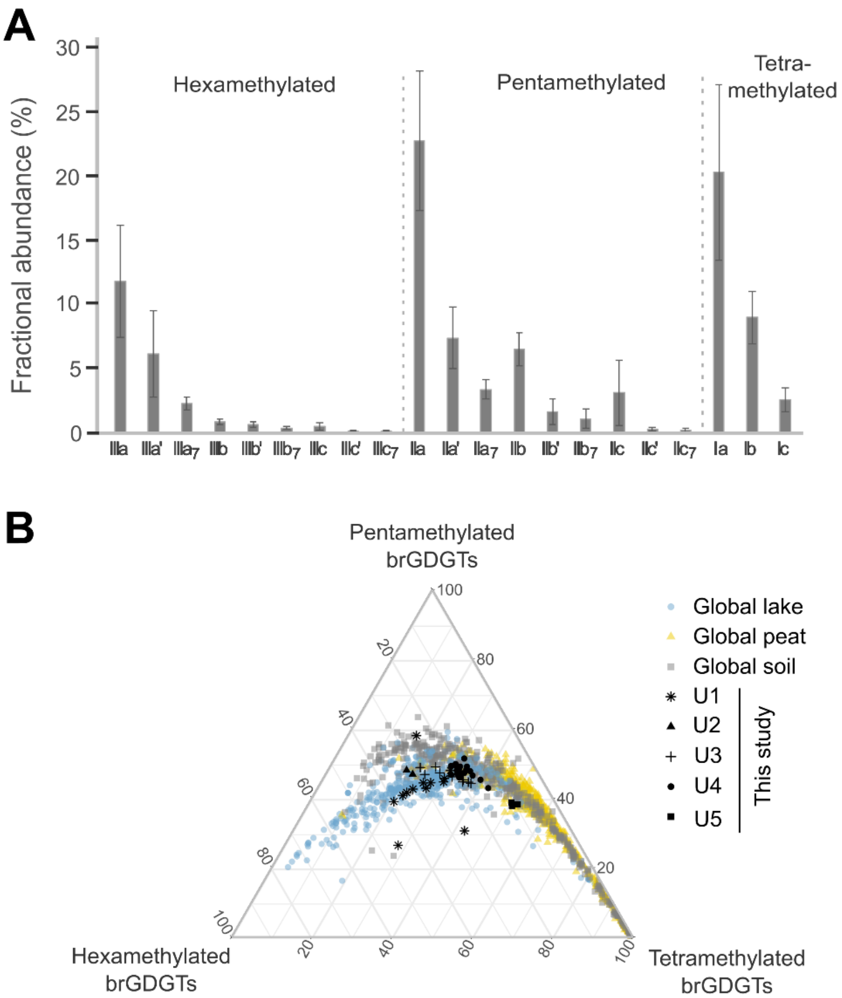

Figure 6. A) Fractional abundance of tetra-, penta-, and hexamethylated brGDGTs for Matese core. B) Ternary diagram showing the fractional abundances of the tetra-, penta-, and hexamethylated brGDGTs for Matese core (black points) and global lake (blue points; Martínez-Sosa et al., 2021), peat (yellow circles; Naafs et al., 2017a), and soils (gray circles; Yang et al., 2014; Naafs et al., 2017b).

4.3.2 Indices of brGDGTs

The relative abundance of tetra-, penta-, and hexamethylated brGDGTs changes along Matese core (Fig. 7). The fractional abundance shows a dominance of pentamethylated brGDGTs except at 518 cm depth, and during the last phase (Phase 4). The fractional abundance of hexamethylated brGDGTs shows higher values between 535-502 cm and 490-466 cm and becomes dominant at 486 cm. The fractional abundance of tetramethylated brGDGTs shows higher values between 502-490 cm and 466-352 cm and is dominant at 518 cm and 352-338 cm (Phase 4).

The degree of methylation (MBT, MBT'$_{5Me}$) and the cyclisation ratio (CBT) also shows variation along Matese core (Fig. 7). The MBT and the MBT'$_{5Me}$ show similar trends but different absolute values; they vary between 0.17 and 0.52 and between 0.20 and 0.63, respectively. The degree of methylation remains relatively stable except during two phases of decrease between 534-522 cm and 486-458 cm, and two phases with higher values at 518 cm depth and during the Phase 4. The CBT varies between 0.27 and 0.74. Phase 1 (535-530 cm) is characterized by high values of CBT following by a decline until reaching a minimum between 494-482 cm. Then, the CBT slightly increases; at 382 cm a slow decline is recorded, and a strong increase marks Phase 4.

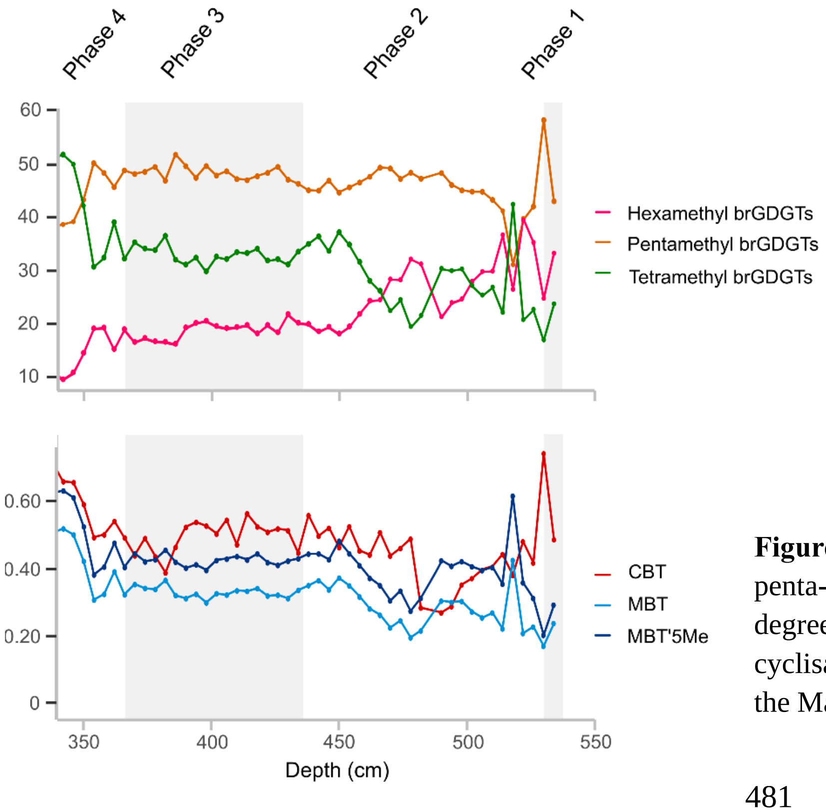

Figure 7. Fractional abundance of tetra-, penta-, and hexamethylated brGDGTs degree of methylation (MBT, MBT'$_{5Me}$), cyclisation ratio (CBT) against depth for the Matese core.

4.3.3 Temperature reconstructions based on brGDGTs

The brGDGT inferred reconstructed MAAT using global (Sun et al., 2011) and East African (Russell et al., 2018) lacustrine calibrations show similar trends than MAF reconstructed using a Bayesian statistical model (Martínez-Sosa et al., 2021) and global (Raberg et al., 2021) lacustrine calibrations (Fig. 8). The values are higher than modern values, especially the values for the MAF_{Full} (Raberg et al., 2021). During Phase 1 (535-530 cm; 14,600-14,500 cal BP), all calibrations show cold temperatures. Phase 2 (530-436 cm; 14,500-12,800 cal BP) is marked by an abrupt temperature increase or a stabilization for MAF_{Meth} or a decline for MAF_{Full}. Between 13,700 and 13,200 cal BP, lower temperatures are recorded with all calibrations and from 13,100 cal BP, temperatures slowly decrease until 11,300 cal BP although a slight increase is recorded between 11,900-11,500 cal BP. Phase 4 (367-338 cm; 11,570-11,000 cal BP) is characterized by a significant increase of temperature.

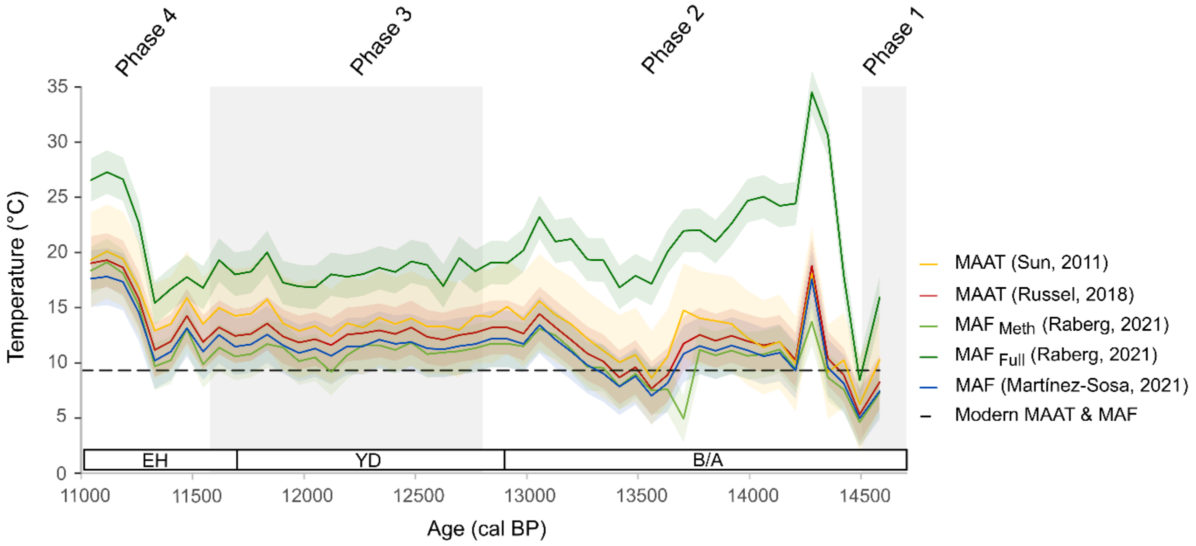

Figure 8. Mean Annual Air Temperature (MAAT) based on global (Sun et al., 2011) and East African (Russell et al., 2018) lacustrine calibrations and Mean temperature of Months Above Freezing (MAF) based on Bayesian statistics (Martínez-Sosa et al., 2021) and global (Raberg et al., 2021) lacustrine calibrations against age for the Matese core. Shaded areas correspond to the error associated with calibrations and **dashed** lines correspond to modern climate values of Lake Matese. **B/A: Bølling–Allerød. YD: Younger Dryas. EH: Early Holocene.**

5. Discussion

5.1 Validation of age-depth model

The compilation of ages derived from the Italian pollen stratigraphy into the Matese age-model is based on the main vegetation changes identified in the area during the Lateglacial. In summary, the OD in Italian pollen records (and in the present study, Fig. 4) is characterized by an open vegetation dominated by Poaceae, *Artemisia,* with a few arboreal pollen such as *Pinus* and *Juniperus* appearing (Allen et al., 2002; Vescovi et al., 2010; Drescher-Schneider et al., 2007; De Beaulieu et al., 2017; Sadori, 2018). During the B/A, a significant increase of arboreal pollen taxa, including deciduous *Quercus* deciduous, is recorded, and in the majority of records *Betula* appears (Allen et al., 2002; Drescher-Schneider et al., 2007; Vescovi et al., 2010; Sadori, 2018; this study). During the YD, an increase of Poaceae and *Artemisia* (Allen et al., 2002; Mercuri et al., 2002; Drescher-Schneider et al., 2007; Vescovi et al., 2010) and an overall decrease of arboreal pollen taxa, except in Southern Italy, (Allen et al., 2002; Beaulieu et al., 2017; this study) are documented.

The ages of tephra samples and ages constrained from the pollen stratigraphy are in good agreement, contrasting results from the ^{14}C dates which are randomly scattered and systematically too young (Fig. 2). The sediments of the Matese core are mainly composed of clay with only few plant fibers. Considering the recurrence of radiocarbon dates between 7570 and 7850 cal BP in the core interval between 420 and 360 cm depth (see Table 1), it is hypothesized that the dated organic matter may have **partly** originated from penetrating **rootlets** of plants growing during sedimentary Unit 5's deposition (Fig. 4). Indeed, aquatic plants of sedimentary Unit 5, identified with pollen, evidence a shallow water body and the development of tree species that typically grow in wetland.

Therefore, the overall age-depth model of the Matese core is based on imported, well-accepted tephra ages and one ^{14}C date of a bulk sediment sample from the bottom of the core at 534 cm (Fig. 2).

5.2 Influence of proxies and methods on climate reconstructions

5.2.1 Lake Matese climate signal reliability

Climate reconstructions are based both on pollen and brGDGTs, and some temperature discrepancies (absolute values or amplitudes) are depicted depending on the proxies (Fig. 9). The temperature amplitudes and absolute values are higher for brGDGTs (5-20°C) than the pollen (4-10°C) reconstructions. Pollen-inferred temperature values depend heavily on the quality of the modern pollen dataset including the number of samples, the diversity of samples in terms of biomes, and the similarity with the fossil samples (Chevalier et al., 2020). In our study, the modern database includes several modern samples from the Matese massif, and 95 samples from Italy were added to complete the dataset. Moreover, the spatial autocorrelation is low for MAT (Moran's $I<0.34$, $p\text{-value}<0.01$), and climate trends are consistent between methods. Reconstructed values for temperatures are close to modern values during the warmest periods, however, precipitation is largely underestimated by all methods for the recent time period (Fig. 5). The same observation was made in Calabria in Southern Italy (Trifoglietti; Joannin et al., 2012), a region also characterized by precipitation above 1700 mm. The underestimation of precipitation is certainly linked to the lack of modern samples located in very wet Mediterranean areas. Considering the brGDGT climate signal, the reconstructed temperatures are overestimated in comparison with modern values (Fig. 8). For shallow temperate lakes (< 20 m), like Lake Matese, our brGDGT reconstructions suggest values anomalously higher than the expected temperature due to thermal variability (seasonal and diurnal; Martínez-Sosa et al., 2021). Lake Matese is located at an altitude of 1012 m a.s.l. and the strong seasonal variability may have influenced the brGDGT distribution. Moreover, the Lake Matese climate reconstructions are based on several global lacustrine calibration datasets, which may not be well adapted to reconstruct paleotemperatures in the Mediterranean region. According to Dugerdil et al. (2021a), local calibrations perform better to reconstruct more reliable absolute values. Unfortunately, at date, only a few global lacustrine calibrations are available, and a local calibration dataset for the Mediterranean region is still missing.

5.2.2 Regional climate signal reliability depending on the proxy

Climate reconstructions inferred from Lake Matese are compared to key terrestrial and marine temperature and precipitation records (Fig. 9, 10) in a latitudinal transect in central Mediterranean. These reconstructions for the Mediterranean region are based on different proxies. Most of those are indicators of annual temperatures, but some of them are indicators of seasonal temperature changes. For example, transfer functions based on chironomid assemblages provide estimates of mean July air temperatures (Larocque and Finsinger, 2008; Heiri et al., 2014; Samartin et al., 2017), while ostracod assemblages allow quantitative reconstruction of both January and July palaeotemperatures (Marchegiano et al., 2020). Planktonic foraminifera provide estimates of spring and autumn sea surface temperatures (SST) (Sicre et al., 2013). **Depending on the production and deposition settings,** molecular biomarkers are considered as indicators **of annual or seasonal** temperatures like brGDGTs or alkenones **(Sbaffi et al., 2004; Sicre et al., 2013; Zhang et al., 2013; Max et al., 2020; Martínez-Sosa et al., 2021; this study).** For precipitation (Fig. 10), fewer reconstructions are available and they are mainly based on records of pollen (Combourieu-Nebout et al., 2013), δ^{18}O *G. bulloides* in marine sediments (Sicre et al., 2013), and δ^{18}O in speleothems (Regattieri et al., 2014). Pollen enable the reconstruction of both annual and seasonal temperatures and precipitation (e.g. Allen et al., 2002; Tarroso et al., 2016).

The comparison between climate reconstructions inferred from different proxies allows us to identify reliable regional climate signals and to reduce the bias linked to each proxy. Indeed, differences may appear for the timing or amplitudes of changes according to the type of proxy. These differences may be amplified by the proxy provenance, either marine or continental. In Figure 9, the temperature reconstructions above 42°N are mainly based on chironomids, and the climate signal reconstructed is consistent between the sites. In South Italy, at Monticchio, climate reconstructions are based on three pollen records from the same site and differences in terms of amplitude and trend are clearly evidenced (Fig. 9I). These differences are linked to the differences in the core location in the lake and the pollen sample resolution (Allen et al., 2002). The closer the core to the center of the lake (dark blue, Fig. 9I), the better the regional vegetation record and therewith a possible regional climate signal (Peyron et al., 2005). Between latitude 41°N and 36°N, sea-surface temperatures (SSTs) were reconstructed from foraminifera and/or alkenones analyzed from marine cores (Sbaffi et al., 2004; Sicre et al., 2013). Alkenone-based SSTs show a low amplitude of 2-3°C between the B/A and the YD periods, whereas foraminifera-based reconstruction of seasonal temperature show differences of 5-10°C between the B/A and the YD. The differences are linked to their respective methods: For alkenones, the estimation of SSTs are based on the molecular biomarker as the C_{37} alkenone unsaturation ($U_{37}^{K\prime}$), whereas, for foraminifera, they are calculated with the MAT method and depend on the occurrence of modern analogues (Sicre et al., 2013).

5.3 Climate changes during the Lateglacial in Italy

5.3.1 Bølling–Allerød warming

The age of transition between the OD and the Bølling–Allerød Interstadial is estimated at around 14,700 cal BP based on the NGRIP ice-core chronology (Rasmussen et al., 2014). In Italy, an abrupt warming is evidenced at ca 14,700 cal BP (Fig. 9). The differences between the different reconstructions seem related to the type of proxy used rather than latitude. The transition is not obvious in the temperature reconstructions based on alkenones (Fig. 9MO; Sbaffi et al., 2004; Sicre et al., 2013), whereas it is well marked in reconstructions based on foraminifera (Fig. 9N; Sicre et al., 2013) and pollen assemblages (Desprat et al., 2013) from the same cores. According to Sicre et al. (2013), alkenones-inferred SSTs could be biased during the Early deglaciation due to water stratification inducing warming of the thin surface water layers where small size nanophytoplankton grow. Except for temperature reconstructions based on alkenones, all the records show an increase of the temperature at the transition OD-B/A (Larocque and Finsinger, 2008; Sicre et al., 2013; Heiri et al., 2014; Marchegiano et al., 2020). The transition, although marked, seems more progressive in the Italian records than in Greenland ice-core but the low resolution of some records can favor this trend. In terms of precipitation (Fig. 10), few records are available in Italy but no significant changes are recorded around 14,700 cal BP by $\delta^{18}O$ *G. bulloides* (Sicre et al., 2013) and pollen transfer functions (Desprat et al., 2013; this study).

The Bølling–Allerød interstadial is a warm interstadial period interrupted by several cold climate oscillations (Rasmussen et al., 2014). According to the synthesis by Moreno et al.

(2014), the Bølling was cooler than the Allerød in the Southern Mediterranean compared to the warmer Northern Mediterranean. In Italy, above 42°N, temperature trends are complex to interpret: some records show an increase of temperature (Fig. 9B; Heiri et al., 2014) whereas other records show a decline (Fig. 9CE; Larocque and Finsinger, 2008; Marchegiano et al., 2020). At Matese, pollen and brGDGTs inferred temperatures decrease (Fig. 9F-H), whereas in the southern part of Italy, there are no significant changes during the B/A (Fig. 9I-O; Allen et al., 2002; Sbaffi et al., 2004; Sicre et al., 2013). Temperature reconstructions in Italy show no distinct difference between the Bølling and the Allerød with respect to the latitude. In terms of amplitude, several studies (Renssen and Isarin, 2001; Heiri et al., 2014; Moreno et al., 2014) suggests that there were less contrasts in temperatures during the B/A in Southern Europe in comparison with Northern Europe. Once again, this difference is not clear in Italy (Fig. 9). At Matese, a significant decrease of brGDGTs-inferred temperature is recorded at 13,700-13,200 cal BP cal BP (Fig. 9H). This change could be attributed to a colder period such as the Older Dryas or the Inter-Allerød cold period, two short periods characterized by colder conditions in the Greenland ice-core records at 14,000 and 13,100 cal BP, respectively (Rasmussen et al., 2014). However, this cooling event do not appear at the same time in the Matese climate curve based on pollen, and it is only vaguely recorded in other Italian records (Fig. 9). We suggest that this change could be attributed to changes of local conditions that are visible in a lithology change (sedimentary Unit 2, Fig. 4). Indeed, brGDGT distribution and origin can differ according to the type of wetland, water level or vegetation changes (Martínez-Sosa et al., 2021; Robles et al., 2022). In terms of precipitation (Fig. 10), no significant changes occur during the B/A in Italy as suggested previously by Renssen and Isarin (2001) for Southern Europe. The Alpine region seems instead to record wetter conditions during the B/A (Barton et al., 2018; Li et al., 2021).

5.3.2 A marked Younger Dryas cold event throughout Italy

The onset of the YD is estimated around 12,900 cal BP according to the Greenland ice-core chronology (Rasmussen et al., 2014). In Italy, above 42°N, the transition between the B/A and the YD is progressive in terms of temperatures except for chironomid records (Fig. 9B; Heiri et al., 2014). At Matese, pollen-based reconstructions show a progressive decline of temperatures with all methods except the MAT (Fig. 9FG). For this method, the transition is more abrupt, but this difference can be attributed to the application of the biome constraint. BrGDGT-based reconstructions record a steady decrease during the YD or no significant changes according to the calibrations used (Fig. 9H). For southern Italian records, the transition is more abrupt and particularly marked in the foraminifera record in contrast to alkenones-based reconstructions (Fig. 9J-O; Sbaffi et al., 2004; Sicre et al., 2013). In terms of precipitation (Fig. 10), the northern Italian speleothems records show an abrupt transition (Regattieri et al., 2014; Li et al., 2021) whereas the southern Italian pollen and isotopes records do not reveal significant changes (Sicre et al., 2013; Combourieu-Nebout et al., 2013; Desprat et al., 2013).

The YD is characterized by cold conditions in the Northern Hemisphere from 12,900 to 11,700 cal BP (Rasmussen et al., 2014). As previously mentioned for the B/A, several studies (Renssen and Isarin, 2001; Heiri et al., 2014; Moreno et al., 2014) suggest that temperatures during the YD are less contrasted in the South of Europe in comparison with the North. In Italy as a whole (Fig. 9), a decline in temperatures is recorded in all records.

At Matese, a decrease of temperatures is evidenced by the pollen-based reconstructions, but it is less clear from the brGDGT-based reconstructions. The difference of climate signals may be related to different sources between both proxies. Pollen record local, extra-local and regional vegetation (Jacobson and Bradshaw, 1981). The basin size of the Lake Matese is larger than 5 hectares, which suggest a signal of regional vegetation rather than local (Jacobson and Bradshaw, 1981). Moreover, the YD is marked by a large proportion of herbaceous taxa (Fig. 4) and favors the catching of regional pollen (Jacobson and Bradshaw, 1981). **By contrast,** brGDGTs are produced in the lake or in the catchment area (Russell et al., 2018; Martin et al., 2019) and thus are local contributors. Moreover, the YD is characterized by high erosion rates in the catchment (Fig. 4), which could favor greater soil-derived brGDGTs and induce a warm bias in temperatures (Martínez-Sosa et al., 2021). Indeed, **the distribution of brGDGTs differ according to sample type and could differ between lake sediments and catchment soils (Loomis et al., 2011, 2014; Buckles et al., 2014; Russell et al., 2018; Martin et al., 2019; Martínez-Sosa et al., 2021; Raberg et al., 2022). Soil sediments generally exhibit less hexamethylated brGDGTs and more tetramethylated brGDGTs than lake sediments (Loomis et al., 2011, 2014; Buckles et al., 2014; Russell et al., 2018; Martin et al., 2019; Martínez-Sosa et al., 2021). However, an increase of tetramethylated brGDGTs is mainly associated with an increase in temperatures in soils and lake sediments (Russell et al., 2018). At Matese, the YD is characterized by a decrease in hexamethylated brGDGTs and a slight increase in tetramethylated brGDGTs. These differences may have affected the annual temperature reconstructions by inducing a warm bias in temperatures during the YD. Furthermore, soil-derived brGDGTs may also be affected by changes in pH, moisture, soil compounds and vegetation in the catchment of Lake Matese (Davtian et al., 2016; Martin et al., 2019; Liang et al., 2019; Dugerdil et al., 2021a). Furthermore soil samples**

without vegetation cover are more sensitive to seasonal changes than that of soil samples with grass and forest cover (Liang et al., 2019). Therefore, soils with vegetation cover allow a better reconstruction of global temperatures (Liang et al., 2019). Since at Matese, the YD is characterized by an open vegetation, soil-derived brGDGTs could also have been affected by seasonal temperature changes due to a sparse vegetation and this effect is superimposed to changes in the sources of brGDGTs in lake sediments.

Contrasted patterns are also recorded at Monticchio (Fig. 9I) by the three different climate variables used for pollen-based temperature reconstructions: a decrease in winter temperature is reconstructed for two lake cores, while a fen core external to the lake, which should record the local vegetation signal, does not reveal the temperature decline during the YD (Allen et al., 2002). However, the two other cores clearly show a temperature decrease, that is why we consider a winter temperature decrease during the YD at Monticchio. In Southern Italian records, temperature reconstructions based on alkenones, foraminifera and pollen (Sbaffi et al., 2004; Desprat et al., 2013; Sicre et al., 2013) show a shorter YD than in the north. For alkenones-based reconstructions, even an increase of temperatures is recorded at the end of the YD. In continental records of South Italy (Allen et al., 2002), this trend is only recorded at Monticchio (one core only) and does not **appear** at Matese. Nonetheless, this hypothesis is only based on marine records and should be investigated through continental records in Southern Italy.

In terms of precipitation, the marine **sequences** located south of latitude 42°N record a slight increase **for proxies** based on pollen (Fig. 9GH; Combourieu-Nebout et al., 2013) and on $\delta^{18}O$ *G. bulloides* data (Fig. 9FI; Sicre et al., 2013) during the YD. However, no significant change occurs at Matese for PANN (Fig. 10D), and on the contrary a low decline is recorded for P_{winter} towards the end of the YD (Fig. 10E). Above latitude 42°N, a precipitation decrease during the YD is recorded by two sites at Hölloch and Corchia caves (Fig. 10BC; Regattieri et al., 2014; Li et al., 2021). According to the model outputs of Rea et al. (2020), drier conditions occurred in Northern Europe whereas wetter conditions prevailed in Southern Europe, mainly during winter and in the South of Italy, the Dinaric Alps and Northern Turkey. This pattern is consistent with our reconstruction but the limit between the North and the South is closer to latitude 42°N.

The transition between the YD and the Holocene is recorded around 11,700 cal BP by Greenland ice-core records (Rasmussen et al., 2014). In Italy, an important increase of temperature is recorded in all records (Fig. 9) which appears earlier (700-400 years) in southern sites (Sbaffi et al., 2004; Sicre et al., 2013). In terms of precipitation, marine records south of latitude 42°N continue to record a slight increase of precipitation (Fig. 10F-I; Combourieu-Nebout et al., 2013; Sicre et al., 2013), and in northern sites an increase of precipitation is recorded (Fig. 10B-E; Regattieri et al., 2014; Li et al., 2021; this study).

5.4 Atmospheric processes during the Lateglacial in central Mediterranean

According to several studies, climate changes during the Lateglacial show differences in temperatures between Southern and Central Europe (Heiri et al., 2014; Moreno et al., 2014; Renssen and Isarin, 2001). In Italy (Fig. 9), climate reconstructions do not show latitudinal differences in terms of temperature. The B/A is marked by warm conditions and the YD by cold conditions even in Southern Italy. Climate reconstructions **for East-Central Southern Europe** from Heiri et al., (2014) are not consistent with our results probably because **while two of their chironomid records are located in North Italy and one in Bulgaria none consider Southern Italy.** In the study of Moreno et al. (2014), only the record of Monticchio is used for the South of Italy during the Lateglacial, which may explain the differences in our study. Considering precipitation, several studies suggest no significant changes during the B/A but drier conditions in Northern Europe and wetter conditions in Southern Europe during the YD. In Italy (Fig. 10), we observe the same dynamics during the B/A and the YD.

Several studies (Renssen and Isarin, 2001; Moreno et al., 2014; Rea et al., 2020) explain that during cold periods of the Lateglacial (OD, YD) the Polar Frontal JetStream moved southward with a weak Atlantic Meridional Overturning Circulation (AMOC) (Moreno et al., 2014; Rea et al., 2020; Renssen and Isarin, 2001). The incursion of cold air masses is recorded until the South of Italy, however, during the YD, dry conditions are not reconstructed **for** this region. According to Rea et al. (2020), a relocation of Atlantic storm tracks **in** the Mediterranean is induced by the Fennoscandian ice sheet and the North European Plain which created a topographic barrier and a high pressure region during the YD. The presence of Atlantic storm tracks into the Mediterranean could have favored wetter conditions in the South of Italy during the YD. Our study suggests a limit around latitude 42°N**,** with drier conditions in Northern Italy and slightly wetter conditions in Southern Italy during the YD. A latitude limit at 40°N was previously discussed by Magny et al. (2013) for the Holocene. These echoing limits over time in Italy inevitably reinforce Italy's key position to archive proxies catching atmospheric patterns.

By contrast, during the B/A, the North Atlantic sea-ice has a more northerly position inducing a northward shift of the Polar Frontal JetStream (Renssen and Isarin, 2001). The incursion of warm air masses is recorded in all of Italy, however, no significant changes in annual precipitation occur. Our study does not suggest the location of Atlantic storm tracks in Italy during the B/A, although at Matese winter precipitation was higher in most pollen-based climate reconstructions. However, very few records and climatic models reconstructing precipitation are available in Europe and the Mediterranean region for this period. Further investigations are necessary to fully understand the atmospheric processes and precipitation dynamic in Europe, mainly during the B/A.

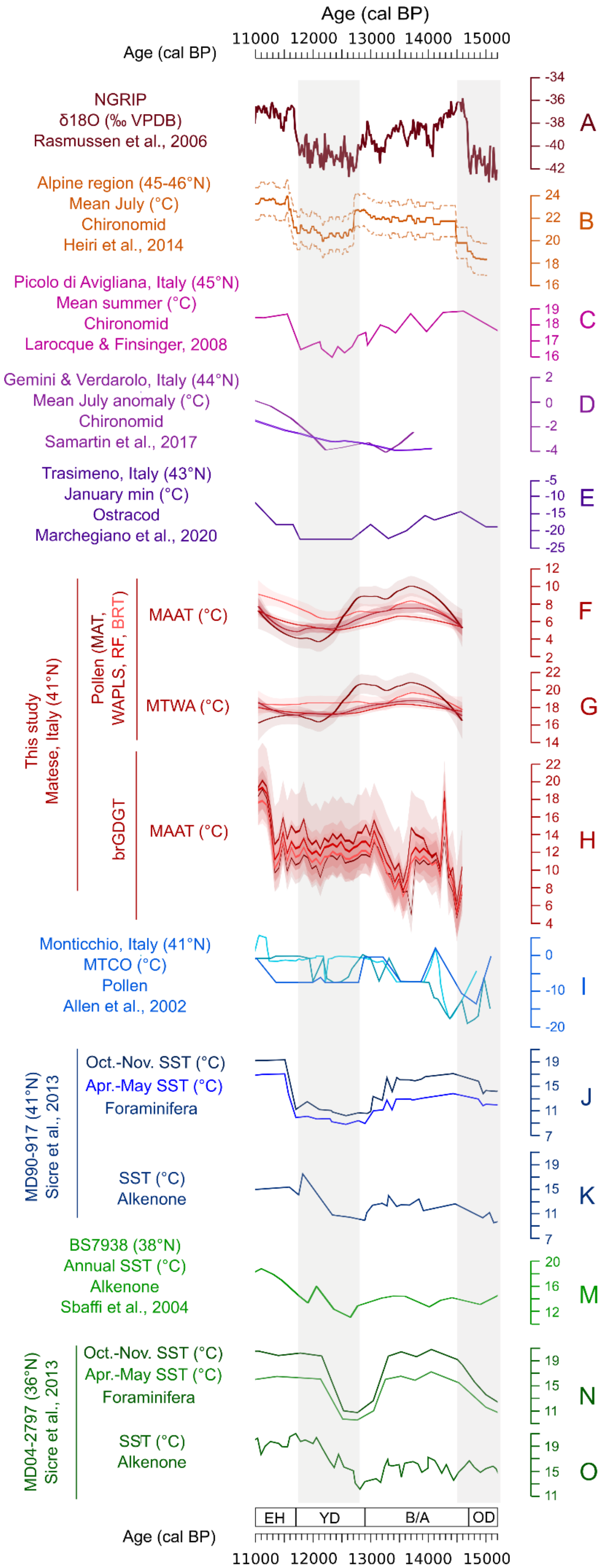
Age (cal BP)
11000 12000 13000 14000 15000
Age (cal BP)
NGRIP
δ18O (‰ VPDB)
Rasmussen et al., 2006
-34 -36 -38 -40 -42
A
Alpine region (45-46°N)
Mean July (°C)
Chironomid
Heiri et al., 2014
24 22 20 18 16
B
Picolo di Avigliana, Italy (45°N)
Mean summer (°C)
Chironomid
Larocque & Finsinger, 2008
19 18 17 16
C
Gemini & Verdarolo, Italy (44°N)
Mean July anomaly (°C)
Chironomid
Samartin et al., 2017
2 0 -2 -4
D
Trasimeno, Italy (43°N)
January min (°C)
Ostracod
Marchegiano et al., 2020
-5 -10 -15 -20 -25
E
This study
Matese, Italy (41°N)
Pollen (MAT, WAPLS, RF, BRT)
MAAT (°C)
12 10 8 6 4 2
F
MTWA (°C)
22 20 18 16 14
G
brGDGT
MAAT (°C)
22 20 18 16 14 12 10 8 6 4
H
Monticchio, Italy (41°N)
MTCO (°C)
Pollen
Allen et al., 2002
0 -10 -20
I
MD90-917 (41°N)
Sicre et al., 2013
Oct.-Nov. SST (°C)
Apr.-May SST (°C)
Foraminifera
19 15 11 7
J
SST (°C)
Alkenone
19 15 11 7
K
BS7938 (38°N)
Annual SST (°C)
Alkenone
Sbaffi et al., 2004
20 16 12
M
MD04-2797 (36°N)
Sicre et al., 2013
Oct.-Nov. SST (°C)
Apr.-May SST (°C)
Foraminifera
19 15 11
N
SST (°C)
Alkenone
19 15 11
O
EH YD B/A OD
Age (cal BP)
11000 12000 13000 14000 15000

Figure 9. Synthesis of temperature records inferred from different proxies in Italy from 15,000 to 11,000 cal BP and comparison with the NGRIP ice core record. MAAT: mean annual air temperature. MTWA: mean temperature of the warmest month. MTCO: mean temperature of the coldest month. OD: Oldest Dryas. B/A: Bølling–Allerød. YD: Younger Dryas. EH: Early Holocene.

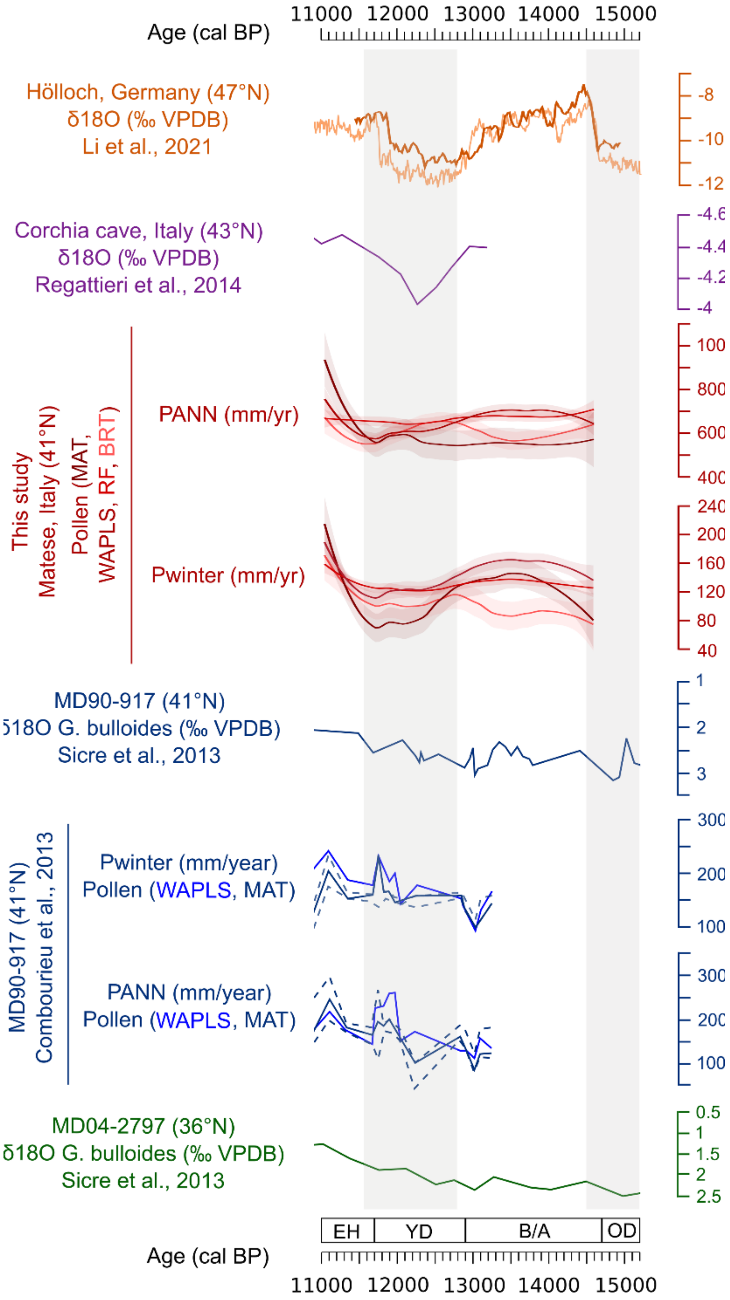

Figure 10. Synthesis of precipitation records inferred from different proxies in Italy 15,000 to 11,000 cal BP. PANN: mean annual precipitation. P_{winter}: winter precipitation. OD: Oldest Dryas. B/A: Bølling–Allerød. YD: Younger Dryas. EH: Early Holocene.

6. Conclusions

This study provides a quantitative climate reconstruction for the Lateglacial period in **Central-Southern** Europe, inferred from a multi-proxy and multi-method approach based on the Lake Matese record. The comparison of the Lake Matese climate reconstructions based on brGDGTs and pollen and their comparison with regional terrestrial/marine climate reconstructions show the following:

- For the first time, pollen and brGDGTs were combined to reconstruct climate changes in the Mediterranean region during the Lateglacial. Temperature trends reconstructed with these proxies are consistent except during the YD. Both proxies show a marked cold OD, an increase of temperatures during the B/A, and an abrupt transition to warmer conditions for the Holocene. During the YD, pollen-based reconstructions show a decrease of temperatures, whereas brGDGT-based reconstructions show no significant changes.
- Comparison with regional climate records of Italy reveals that there are no latitudinal differences during the B/A and the YD in terms of temperatures. The B/A is marked by an increase of temperature and the YD is characterized by cold conditions in all Italy. **By contrast**, precipitation does not show changes during the B/A, and a slight increase of precipitation during the YD is recorded in Southern Italy below latitude 42°N.
- Cold conditions during the YD in Italy may be linked to the southward position of North Atlantic sea-ice and of the Polar Frontal JetStream. The low increase of precipitation during the YD may be linked to relocation of Atlantic storm tracks into the Mediterranean, induced by the Fennoscandian ice sheet and the North European Plain. We identified the latitude 42°N as a limit between dry conditions in northern Italy and slightly wetter conditions in Southern Italy during the YD. **By contrast**, warm conditions during the B/A may be linked to the northward position of North Atlantic sea-ice and of the Polar Frontal JetStream.

In summary, this study allowed us to document and discuss past climate changes in Italy while contributing to the debate about the atmospheric processes in Southern Europe. The latitudes 40-42°N appear as a key junction point between wetter conditions in Southern Italy and drier conditions in Northern Italy during the YD but also during the Early-Mid Holocene (Magny et al., 2013). However, further robust paleoclimate studies are needed to provide 1) high-resolution reconstructions based on several proxies in Northern Italy, 2) new records for central Italy (between 41-43°N), 3) new continental records for Southern Italy (below 41°N) and 4) more model outputs at regional scales with transient simulations, if possible, mainly during the B/A and the YD.

Author contribution

MR: Conceptualization, Field work, Laboratory work, Formal analysis, Writing draft manuscript, Review, Funding acquisition. SJ, OP and EB: Conceptualization, Field work, Supervision, Review, Funding acquisition. GM: Conceptualization, Supervision, Review, Funding acquisition. SW: Laboratory work, Formal analysis, Review, Funding acquisition. OA and MB: Laboratory work. BV: Supervision of laboratory work, Review. BP: Field work. SAA: Coordination of laboratory work. LC and SG: Conceptualization, Review. J-LB, LD and AC: Review.

Declaration of competing interest

The authors declare that they have no known competing financial interests or personal relationships that could have appeared to influence the work reported in this paper.

Funding

This research was co-founded by the International PhD course "Agriculture Technologies and Biotechnologies" (34° Cycle, Code: DOT1339335). Financial support for this study was provided by EFFICACE project from EC2CO INSU CNRS (PI: Odile Peyron) and ERJ ClimMatese from LabEx CeMEB (PI: Mary Robles). The travels between Italy and France were financed by VINCI founding of the Università Italo Francese (UIF). The conference funding was provided by the Association des Palynologues de Langue Française (APLF).

Acknowledgements

The authors would like to thank Julien Didier for magnetic susceptibility measurements, Laurent Bouby and Isabelle Figueral for seed and wood identifications used for radiocarbon dating. The authors would like to express their appreciation to Gwenaël Magne, Thierry Pastor and Benoît Brossier for logistical support during fieldwork, and Anne-Lise Develle and Claire Blanchet for help during XRF analysis. We would like to thank Sandrine Canal and Sylvie

Rouland for support during pollen sample preparation. This is an ISEM contribution N° XXXX-XXX.

References

Allen, J.R.M., Watts, W.A., McGee, E., Huntley, B., 2002. Holocene environmental variability-the record from Lago Grande di Monticchio, Italy. Quaternary International 88, 69–80.

Ammann, B., Birks, H.J.B., Brooks, S.J., Eicher, U., von Grafenstein, U., Hofmann, W., Lemdahl, G., Schwander, J., Tobolski, K., Wick, L., 2000. Quantification of biotic responses to rapid climatic changes around the Younger Dryas — a synthesis. Palaeogeography, Palaeoclimatology, Palaeoecology 159, 313–347. https://doi.org/10.1016/S0031-0182(00)00092-4

Aucelli, P.P.C., Cesarano, M., Di Paola, G., Filocamo, F., Rosskopf, C.M., 2013. Geomorphological map of the central sector of the Matese Mountains (Southern Italy): an example of complex landscape evolution in a Mediterranean mountain environment. Journal of Maps 9, 604–616. https://doi.org/10.1080/17445647.2013.840054

Barton, C.M., Aura Tortosa, J.E., Garcia-Puchol, O., Riel-Salvatore, J.G., Gauthier, N., Vadillo Conesa, M., Pothier Bouchard, G., 2018. Risk and resilience in the late glacial: A case study from the western Mediterranean. Quaternary Science Reviews 184, 68–84. https://doi.org/10.1016/j.quascirev.2017.09.015

Beug, H.-J., 2004. Leitfaden der Pollenbestimmung für Mitteleuropa und angrenzende Gebiete. Friedrich Pfeil, München.

Blaauw, M., 2010. Methods and code for 'classical' age-modelling of radiocarbon sequences. Quaternary Geochronology 5, 512–518. https://doi.org/10.1016/j.quageo.2010.01.002

Blaga, C.I., Reichart, G.-J., Lotter, A.F., Anselmetti, F.S., Sinninghe Damsté, J.S., 2013. A TEX$_{86}$ lake record suggests simultaneous shifts in temperature in Central Europe and Greenland during the last deglaciation: A SWISS TEX$_{86}$ LAKE RECORD. Geophys. Res. Lett. 40, 948–953. https://doi.org/10.1002/grl.50181

Breiman, L., 2001. Random Forests. Machine Learning 45, 5–32. https://doi.org/10.1023/A:1010933404324

Bronk Ramsey, C., Albert, P.G., Blockley, S.P.E., Hardiman, M., Housley, R.A., Lane, C.S., Lee, S., Matthews, I.P., Smith, V.C., Lowe, J.J., 2015. Improved age estimates for key Late Quaternary European tephra horizons in the RESET lattice. Quaternary Science Reviews 118, 18–32. https://doi.org/10.1016/j.quascirev.2014.11.007

Buckles, L.K., Weijers, J.W.H., Verschuren, D., Sinninghe Damsté, J.S., 2014. Sources of core and intact branched tetraether membrane lipids in the lacustrine environment: Anatomy of Lake Challa and its catchment, equatorial East Africa. Geochimica et Cosmochimica Acta 140, 106–126. https://doi.org/10.1016/j.gca.2014.04.042

Carranza, M.L., Frate, L., Paura, B., 2012. Structure, ecology and plant richness patterns in fragmented beech forests. Plant Ecology & Diversity 5, 541–551. https://doi.org/10.1080/17550874.2012.740509

Castañeda, I.S., Schouten, S., 2011. A review of molecular organic proxies for examining modern and ancient lacustrine environments. Quaternary Science Reviews 30, 2851–2891. https://doi.org/10.1016/j.quascirev.2011.07.009

Chevalier, M., Davis, B.A.S., Heiri, O., Seppä, H., Chase, B.M., Gajewski, K., Lacourse, T., Telford, R.J., Finsinger, W., Guiot, J., Kühl, N., Maezumi, S.Y., Tipton, J.R., Carter, V.A., Brussel, T., Phelps, L.N., Dawson, A., Zanon, M., Vallé, F., Nolan, C., Mauri, A., de Vernal, A., Izumi, K., Holmström, L., Marsicek, J., Goring, S., Sommer, P.S., Chaput, M., Kupriyanov, D., 2020. Pollen-based climate reconstruction techniques for late Quaternary studies. Earth-Science Reviews 210, 103384. https://doi.org/10.1016/j.earscirev.2020.103384

Combourieu-Nebout, N., Peyron, O., Bout-Roumazeilles, V., Goring, S., Dormoy, I., Joannin, S., Sadori, L., Siani, G., Magny, M., 2013. Holocene vegetation and climate changes in the central Mediterranean inferred from a high-resolution marine pollen record (Adriatic Sea). Clim. Past 9, 2023–2042. https://doi.org/10.5194/cp-9-2023-2013

Coope, G.R., Lemdahl, G., 1995. Regional differences in the Lateglacial climate of northern Europe based on coleopteran analysis. Journal of Quaternary Science 10, 391–395. https://doi.org/10.1002/jqs.3390100409

Davtian, N., Bard, E., Ménot, G., Fagault, Y., 2018. The importance of mass accuracy in selected ion monitoring analysis of branched and isoprenoid tetraethers. Organic Geochemistry 118, 58–62. https://doi.org/10.1016/j.orggeochem.2018.01.007

Davtian, N., Ménot, G., Bard, E., Poulenard, J., Podwojewski, P., 2016. Consideration of soil types for the calibration of molecular proxies for soil pH and temperature using global soil datasets and Vietnamese soil profiles. Organic Geochemistry 101, 140–153. https://doi.org/10.1016/j.orggeochem.2016.09.002

De Beaulieu, J.-L., Brugiapaglia, E., Joannin, S., Guiter, F., Zanchetta, G., Wulf, S., Peyron, O., Bernardo, L., Didier, J., Stock, A., Rius, D., Magny, M., 2017. Lateglacial-Holocene abrupt vegetation changes at Lago Trifoglietti in Calabria, Southern Italy: The setting of ecosystems in a refugial zone. Quaternary Science Reviews 158, 44–57. https://doi.org/10.1016/j.quascirev.2016.12.013

De Jonge, C., Stadnitskaia, A., Hopmans, E.C., Cherkashov, G., Fedotov, A., Sinninghe Damsté, J.S., 2014. In situ produced branched glycerol dialkyl glycerol tetraethers in suspended particulate matter from the Yenisei River, Eastern Siberia. Geochimica et Cosmochimica Acta 125, 476–491. https://doi.org/10.1016/j.gca.2013.10.031

Dearing Crampton-Flood, E., Tierney, J.E., Peterse, F., Kirkels, F.M.S.A., Sinninghe Damsté, J.S., 2020. BayMBT: A Bayesian calibration model for branched glycerol dialkyl glycerol tetraethers in soils and peats. Geochimica et Cosmochimica Acta 268, 142–159. https://doi.org/10.1016/j.gca.2019.09.043

De'ath, G., 2007. Boosted trees for ecological modeling and prediction. Ecology 88, 243–251. https://doi.org/10.1890/0012-9658(2007)88[243:BTFEMA]2.0.CO;2

Desprat, S., Combourieu-Nebout, N., Essallami, L., Sicre, M.A., Dormoy, I., Peyron, O., Siani, G., Bout Roumazeilles, V., Turon, J.L., 2013. Deglacial and Holocene vegetation and climatic changes in the southern Central Mediterranean from a direct land–sea correlation. Clim. Past 9, 767–787. https://doi.org/10.5194/cp-9-767-2013

Ding, S., Schwab, V.F., Ueberschaar, N., Roth, V.-N., Lange, M., Xu, Y., Gleixner, G., Pohnert, G., 2016. Identification of novel 7-methyl and cyclopentanyl branched glycerol dialkyl glycerol tetraethers in lake sediments. Organic Geochemistry 102, 52–58. https://doi.org/10.1016/j.orggeochem.2016.09.009

Drescher-Schneider, R., de Beaulieu, J.-L., Magny, M., Walter-Simonnet, A.-V., Bossuet, G., Millet, L., Brugiapaglia, E., Drescher, A., 2007. Vegetation history, climate and human impact over the last 15,000 years at Lago dell'Accesa (Tuscany, Central Italy). Veget Hist Archaeobot 16, 279–299. https://doi.org/10.1007/s00334-006-0089-z

Dugerdil, L., Joannin, S., Peyron, O., Jouffroy-Bapicot, I., Vannière, B., Boldgiv, B., Unkelbach, J., Behling, H., Ménot, G., 2021a. Climate reconstructions based on GDGT and pollen surface datasets from Mongolia and Baikal area: calibrations and applicability to extremely cold–dry environments over the Late Holocene. Clim. Past 17, 1199–1226. https://doi.org/10.5194/cp-17-1199-2021

Dugerdil, L., Ménot, G., Peyron, O., Jouffroy-Bapicot, I., Ansanay-Alex, S., Antheaume, I., Behling, H., Boldgiv, B., Develle, A.-L., Grossi, V., Magail, J., Makou, M., Robles, M., Unkelbach, J., Vannière, B., Joannin, S., 2021b. Late Holocene Mongolian climate and environment reconstructions from brGDGTs, NPPs and pollen transfer functions for Lake Ayrag: Paleoclimate implications for Arid Central Asia. Quaternary Science Reviews 273, 107235. https://doi.org/10.1016/j.quascirev.2021.107235

Duprat-Oualid, F., Bégeot, C., Peyron, O., Rius, D., Millet, L., Magny, M., 2022. High-frequency vegetation and climatic changes during the Lateglacial inferred from the Lapsou pollen record (Cantal, southern Massif Central, France). Quaternary International S1040618222001537. https://doi.org/10.1016/j.quaint.2022.04.012

Elith, J., Leathwick, J.R., Hastie, T., 2008. A working guide to boosted regression trees. J Anim Ecology 77, 802–813. https://doi.org/10.1111/j.1365-2656.2008.01390.x

Faegri, K., Kaland, P.E., Krzywinski, K., 1989. Textbook of pollen analysis. John Wiley & Sons, Chichester.

Ferranti, L., Milano, G., Burrato, P., Palano, M., Cannavò, F., 2015. The seismogenic structure of the 2013–2014 Matese seismic sequence, Southern Italy: implication for the geometry of the Apennines active extensional belt. Geophysical Journal International 201, 823–837. https://doi.org/10.1093/gji/ggv053

Ferrarini, F., Boncio, P., de Nardis, R., Pappone, G., Cesarano, M., Aucelli, P.P.C., Lavecchia, G., 2017. Segmentation pattern and structural complexities in seismogenic extensional settings: The North Matese Fault System (Central Italy). Journal of Structural Geology 95, 93–112. https://doi.org/10.1016/j.jsg.2016.11.006

Finsinger, W., Heiri, O., Valsecchi, V., Tinner, W., Lotter, A.F., 2007. Modern pollen assemblages as climate indicators in southern Europe. Global Ecology and Biogeography 16, 567–582. https://doi.org/10.1111/j.1466-8238.2007.00313.x

Fiorillo, F., Doglioni, A., 2010. The relation between karst spring discharge and rainfall by cross-correlation analysis (Campania, southern Italy). Hydrogeol J 18, 1881–1895. https://doi.org/10.1007/s10040-010-0666-1

Fiorillo, F., Pagnozzi, M., 2015. Recharge processes of Matese karst massif (southern Italy). Environ Earth Sci 74, 7557–7570. https://doi.org/10.1007/s12665-015-4678-y

Galli, P., Giaccio, B., Messina, P., Peronace, E., Amato, V., Naso, G., Nomade, S., Pereira, A., Piscitelli, S., Bellanova, J., Billi, A., Blamart, D., Galderisi, A., Giocoli, A., Stabile, T., Thil, F., 2017. Middle to Late Pleistocene activity of the northern Matese fault system (southern Apennines, Italy). Tectonophysics 699, 61–81. https://doi.org/10.1016/j.tecto.2017.01.007

Gandouin, E., Rioual, P., Pailles, C., Brooks, S.J., Ponel, P., Guiter, F., Djamali, M., Andrieu-Ponel, V., Birks, H.J.B., Leydet, M., Belkacem, D., Haas, J.N., Van der Putten, N., de Beaulieu, J.L., 2016. Environmental and climate reconstruction of the late-glacial-Holocene transition from a lake sediment sequence in Aubrac, French Massif Central: Chironomid and diatom evidence. Palaeogeography, Palaeoclimatology, Palaeoecology 461, 292–309. https://doi.org/10.1016/j.palaeo.2016.08.039

Guarino, R., Bazan, G., Paura, B., 2015. Downy-Oak Woods of Italy: Phytogeographical Remarks on a Controversial Taxonomic and Ecologic Issue, in: Box, E.O., Fujiwara, K. (Eds.), Warm-Temperate Deciduous Forests around the Northern Hemisphere, Geobotany Studies. Springer International Publishing, Cham, pp. 139–151. https://doi.org/10.1007/978-3-319-01261-2_7

Guiot, J., 1990. Methodology of the last climatic cycle reconstruction in France from pollen data. Palaeogeography, Palaeoclimatology, Palaeoecology, Methods for the Study of Stratigraphical Records 80, 49–69. https://doi.org/10.1016/0031-0182(90)90033-4

Guiot, J., de Beaulieu, J.L., Cheddadi, R., David, F., Ponel, P., Reille, M., 1993. The climate in Western Europe during the last Glacial/Interglacial cycle derived from pollen and insect remains. Palaeogeography, Palaeoclimatology, Palaeoecology 103, 73–93. https://doi.org/10.1016/0031-0182(93)90053-L

Heiri, O., Brooks, S.J., Renssen, H., Bedford, A., Hazekamp, M., Ilyashuk, B., Jeffers, E.S., Lang, B., Kirilova, E., Kuiper, S., Millet, L., Samartin, S., Toth, M., Verbruggen, F., Watson, J.E., van Asch, N., Lammertsma, E., Amon, L., Birks, H.H., Birks, H.J.B., Mortensen, M.F., Hoek, W.Z., Magyari, E., Muñoz Sobrino, C., Seppä, H., Tinner, W., Tonkov, S., Veski, S., Lotter, A.F., 2014. Validation of climate model-inferred regional temperature change for late-glacial Europe. Nat Commun 5, 4914. https://doi.org/10.1038/ncomms5914

Heiri, O., Ilyashuk, B., Millet, L., Samartin, S., Lotter, A.F., 2015. Stacking of discontinuous regional palaeoclimate records: Chironomid-based summer temperatures from the Alpine region. The Holocene 25, 137–149. https://doi.org/10.1177/0959683614556382

Hepp, J., Wüthrich, L., Bromm, T., Bliedtner, M., Schäfer, I.K., Glaser, B., Rozanski, K., Sirocko, F., Zech, R., Zech, M., 2019. How dry was the Younger Dryas? Evidence from a coupled δ^{2}H–δ^{18}O biomarker paleohygrometer applied to the Gemündener Maar sediments, Western Eifel, Germany. Climate of the Past 15, 713–733. https://doi.org/10.5194/cp-15-713-2019

Hijmans, R.J., Phillips, S., Elith, J.L. and J., 2021. dismo: Species Distribution Modeling.

Hopmans, E.C., Schouten, S., Sinninghe Damsté, J.S., 2016. The effect of improved chromatography on GDGT-based palaeoproxies. Organic Geochemistry 93, 1–6. https://doi.org/10.1016/j.orggeochem.2015.12.006

Huguet, C., Hopmans, E.C., Febo-Ayala, W., Thompson, D.H., Sinninghe Damsté, J.S., Schouten, S., 2006. An improved method to determine the absolute abundance of glycerol dibiphytanyl glycerol tetraether lipids. Organic Geochemistry 37, 1036–1041. https://doi.org/10.1016/j.orggeochem.2006.05.008

Hunt, J.B., Hill, P.G., 1996. An inter-laboratory comparison of the electron probe microanalysis of glass geochemistry. Quaternary International 34–36, 229–241. https://doi.org/10.1016/1040-6182(95)00088-7

Jacobson, G.L., Bradshaw, R.H.W., 1981. The Selection of Sites for Paleovegetational Studies. Quat. res. 16, 80–96. https://doi.org/10.1016/0033-5894(81)90129-0

Joannin, S., Brugiapaglia, E., Vanniere, B., 2012. Pollen-based reconstruction of Holocene vegetation and climate in southern Italy: the case of Lago Trifoglietti. Clim. Past 24.

Jochum, K.P., Stoll, B., Herwig, K., Willbold, M., Hofmann, A.W., Amini, M., Aarburg, S., Abouchami, W., Hellebrand, E., Mocek, B., Raczek, I., Stracke, A., Alard, O., Bouman, C., Becker, S., Dücking, M., Brätz, H., Klemd, R., de Bruin, D., Canil, D., Cornell, D., de Hoog, C.-J., Dalpé, C., Danyushevsky, L., Eisenhauer, A., Gao, Y., Snow, J.E., Groschopf, N., Günther, D., Latkoczy, C., Guillong, M., Hauri, E.H., Höfer, H.E., Lahaye, Y., Horz, K., Jacob, D.E., Kasemann, S.A., Kent, A.J.R., Ludwig, T., Zack, T., Mason, P.R.D., Meixner, A., Rosner, M., Misawa, K., Nash, B.P., Pfänder, J., Premo, W.R., Sun, W.D., Tiepolo, M., Vannucci, R., Vennemann, T., Wayne, D., Woodhead, J.D., 2006. MPI-DING reference glasses for in situ microanalysis: New reference values for element concentrations and isotope ratios: MPI-DING REFERENCE GLASSES. Geochem. Geophys. Geosyst. 7, n/a-n/a. https://doi.org/10.1029/2005GC001060

Juggins, S., Juggins, M.S., 2020. Package ‘rioja.’

Kuehn, S.C., Froese, D.G., Shane, P.A.R., 2011. The INTAV intercomparison of electron-beam microanalysis of glass by tephrochronology laboratories: Results and recommendations. Quaternary International, Enhancing tephrochronology and its application (INTREPID Project): Hiroshi Machida commemorative volume 246, 19–47. https://doi.org/10.1016/j.quaint.2011.08.022

Larocque, I., Finsinger, W., 2008. Late-glacial chironomid-based temperature reconstructions for Lago Piccolo di Avigliana in the southwestern Alps (Italy). Palaeogeography, Palaeoclimatology, Palaeoecology 257, 207–223. https://doi.org/10.1016/j.palaeo.2007.10.021

Li, H., Spötl, C., Cheng, H., 2021. A high-resolution speleothem proxy record of the Late Glacial in the European Alps: extending the NALPS19 record until the beginning of the Holocene. J. Quaternary Sci 36, 29–39. https://doi.org/10.1002/jqs.3255

Liang, J., Russell, J.M., Xie, H., Lupien, R.L., Si, G., Wang, J., Hou, J., Zhang, G., 2019. Vegetation effects on temperature calibrations of branched glycerol dialkyl glycerol tetraether (brGDGTs) in soils. Organic Geochemistry 127, 1–11. https://doi.org/10.1016/j.orggeochem.2018.10.010

Liaw, A., Wiener, M., 2002. Classification and Regression by randomForest 2, 5.

Loomis, S.E., Russell, J.M., Heureux, A.M., D'Andrea, W.J., Sinninghe Damsté, J.S., 2014. Seasonal variability of branched glycerol dialkyl glycerol tetraethers (brGDGTs) in a temperate lake system. Geochimica et Cosmochimica Acta 144, 173–187. https://doi.org/10.1016/j.gca.2014.08.027

Loomis, S.E., Russell, J.M., Sinninghe Damsté, J.S., 2011. Distributions of branched GDGTs in soils and lake sediments from western Uganda: Implications for a lacustrine paleothermometer. Organic Geochemistry 42, 739–751. https://doi.org/10.1016/j.orggeochem.2011.06.004

Lotter, A.F., Heiri, O., Brooks, S., van Leeuwen, J.F.N., Eicher, U., Ammann, B., 2012. Rapid summer temperature changes during Termination 1a: high-resolution multi-proxy climate reconstructions from Gerzensee (Switzerland). Quaternary Science Reviews, The INTegration of Ice core, Marine and TErrestrial records of the last termination (INTIMATE) 60,000 to 8000 BP 36, 103–113. https://doi.org/10.1016/j.quascirev.2010.06.022

Magny, M., Combourieu-Nebout, N., de Beaulieu, J.-L., Bout-Roumazeilles, V., Colombaroli, D., Desprat, S., Francke, A., Joannin, S., Ortu, E., Peyron, O., Revel, M., Sadori, L., Siani, G., Sicre, M.A., Samartin, S., Simonneau, A., Tinner, W., Vanniere, B., Wagner, B., Zanchetta, G., Anselmetti, F., Brugiapaglia, E., Chapron, E., Debret, M., Didier, J., Essallami, L., Galop, D., Gilli, A., Kallel, N., Millet, L., Stock, A., Turon, J.L., Wirth, S., 2013. North-south palaeohydrological contrasts in the central Mediterranean during the Holocene: tentative synthesis and working hypotheses. Clim. Past 30.

Marchegiano, M., Horne, D.J., Gliozzi, E., Francke, A., Wagner, B., Ariztegui, D., 2020. Rapid Late Pleistocene climate change reconstructed from a lacustrine ostracod record in central Italy (Lake Trasimeno, Umbria). Boreas 49, 739–750. https://doi.org/10.1111/bor.12450

Martin, C., Ménot, G., Thouveny, N., Davtian, N., Andrieu-Ponel, V., Reille, M., Bard, E., 2019. Impact of human activities and vegetation changes on the tetraether sources in Lake St Front (Massif Central, France). Organic Geochemistry 135, 38–52.

Martin, C., Ménot, G., Thouveny, N., Peyron, O., Andrieu-Ponel, V., Montade, V., Davtian, N., Reille, M., Bard, E., 2020. Early Holocene Thermal Maximum recorded by branched tetraethers and pollen in Western Europe (Massif Central, France). Quaternary Science Reviews 228, 106109. https://doi.org/10.1016/j.quascirev.2019.106109

Martínez-Sosa, P., Tierney, J.E., Stefanescu, I.C., Dearing Crampton-Flood, E., Shuman, B.N., Routson, C., 2021. A global Bayesian temperature calibration for lacustrine brGDGTs. Geochimica et Cosmochimica Acta 305, 87–105. https://doi.org/10.1016/j.gca.2021.04.038

Max, L., Lembke-Jene, L., Zou, J., Shi, X., Tiedemann, R., 2020. Evaluation of reconstructed sea surface temperatures based on U37k′ from sediment surface samples of the North

Pacific. Quaternary Science Reviews 243, 106496. https://doi.org/10.1016/j.quascirev.2020.106496

Mercuri, A.M., Accorsi, C.A., Bandini Mazzanti, M., 2002. The long history of Cannabis and its cultivation by the Romans in central Italy, shown by pollen records from Lago Albano and Lago di Nemi. Veget Hist Archaeobot 11, 263–276. https://doi.org/10.1007/s003340200039

Millet, L., Rius, D., Galop, D., Heiri, O., Brooks, S.J., 2012. Chironomid-based reconstruction of Lateglacial summer temperatures from the Ech palaeolake record (French western Pyrenees). Palaeogeography, Palaeoclimatology, Palaeoecology 315–316, 86–99. https://doi.org/10.1016/j.palaeo.2011.11.014

Moore, P.D., Webb, J.A., Collinson, M.E., 1991. Pollen Analysis, Subsequent edition. ed. Blackwell Science Inc, Oxford.

Moreno, A., Svensson, A., Brooks, S.J., Connor, S., Engels, S., Fletcher, W., Genty, D., Heiri, O., Labuhn, I., Perşoiu, A., Peyron, O., Sadori, L., Valero-Garcés, B., Wulf, S., Zanchetta, G., 2014. A compilation of Western European terrestrial records 60–8 ka BP: towards an understanding of latitudinal climatic gradients. Quaternary Science Reviews 106, 167–185. https://doi.org/10.1016/j.quascirev.2014.06.030

Naafs, B.D.A., Gallego-Sala, A.V., Inglis, G.N., Pancost, R.D., 2017a. Refining the global branched glycerol dialkyl glycerol tetraether (brGDGT) soil temperature calibration. Organic Geochemistry 106, 48–56. https://doi.org/10.1016/j.orggeochem.2017.01.009

Naafs, B.D.A., Inglis, G.N., Zheng, Y., Amesbury, M.J., Biester, H., Bindler, R., Blewett, J., Burrows, M.A., del Castillo Torres, D., Chambers, F.M., Cohen, A.D., Evershed, R.P., Feakins, S.J., Gałka, M., Gallego-Sala, A., Gandois, L., Gray, D.M., Hatcher, P.G., Honorio Coronado, E.N., Hughes, P.D.M., Huguet, A., Könönen, M., Laggoun-Défarge, F., Lähteenoja, O., Lamentowicz, M., Marchant, R., McClymont, E., Pontevedra-Pombal, X., Ponton, C., Pourmand, A., Rizzuti, A.M., Rochefort, L., Schellekens, J., De Vleeschouwer, F., Pancost, R.D., 2017b. Introducing global peat-specific temperature and pH calibrations based on brGDGT bacterial lipids. Geochimica et Cosmochimica Acta 208, 285–301. https://doi.org/10.1016/j.gca.2017.01.038

Panagiotopoulos, K., Holtvoeth, J., Kouli, K., Marinova, E., Francke, A., Cvetkoska, A., Jovanovska, E., Lacey, J.H., Lyons, E.T., Buckel, C., Bertini, A., Donders, T., Just, J., Leicher, N., Leng, M.J., Melles, M., Pancost, R.D., Sadori, L., Tauber, P., Vogel, H., Wagner, B., Wilke, T., 2020. Insights into the evolution of the young Lake Ohrid ecosystem and vegetation succession from a southern European refugium during the Early Pleistocene. Quaternary Science Reviews 227, 106044. https://doi.org/10.1016/j.quascirev.2019.106044

Peyron, O., Bégeot, C., Brewer, S., Heiri, O., Magny, M., Millet, L., Ruffaldi, P., Van Campo, E., Yu, G., 2005. Late-Glacial climatic changes in Eastern France (Lake Lautrey) from pollen, lake-levels, and chironomids. Quat. res. 64, 197–211. https://doi.org/10.1016/j.yqres.2005.01.006

Peyron, O., Combourieu-Nebout, N., Brayshaw, D., Goring, S., Andrieu-Ponel, V., Desprat, S., Fletcher, W., Gambin, B., Ioakim, C., Joannin, S., Kotthoff, U., Kouli, K., Montade, V., Pross, J., Sadori, L., Magny, M., 2017. Precipitation changes in the Mediterranean basin during the Holocene from terrestrial and marine pollen records: a model–data comparison. Clim. Past 13, 249–265. https://doi.org/10.5194/cp-13-249-2017

Peyron, O., Goring, S., Dormoy, I., Kotthoff, U., Pross, J., de Beaulieu, J.-L., Drescher-Schneider, R., Vannière, B., Magny, M., 2011. Holocene seasonality changes in the central Mediterranean region reconstructed from the pollen sequences of Lake Accesa (Italy) and Tenaghi Philippon (Greece). The Holocene 21, 131–146. https://doi.org/10.1177/0959683610384162

Peyron, O., Guiot, J., Cheddadi, R., Tarasov, P., Reille, M., de Beaulieu, J.-L., Bottema, S., Andrieu, V., 1998. Climatic Reconstruction in Europe for 18,000 YR B.P. from Pollen Data. Quat. res. 49, 183–196. https://doi.org/10.1006/qres.1997.1961

Peyron, O., Magny, M., Goring, S., Joannin, S., de Beaulieu, J.-L., Brugiapaglia, E., Sadori, L., Garfi, G., Kouli, K., Ioakim, C., Combourieu-Nebout, N., 2013. Contrasting patterns of climatic changes during the Holocene across the Italian Peninsula reconstructed from pollen data. Clim. Past 9, 1233–1252. https://doi.org/10.5194/cp-9-1233-2013

Ponel, P., Guiter, F., Gandouin, E., Peyron, O., de Beaulieu, J.-L., 2022. Late-Glacial palaeotemperatures and palaeoprecipitations in the Aubrac Mountains (French Massif Central) reconstructed from multiproxy analyses (Coleoptera, chironomids and pollen). Quaternary International. https://doi.org/10.1016/j.quaint.2022.02.005

Prasad, A.M., Iverson, L.R., Liaw, A., 2006. Newer Classification and Regression Tree Techniques: Bagging and Random Forests for Ecological Prediction. Ecosystems 9, 181–199. https://doi.org/10.1007/s10021-005-0054-1

Prentice, C., Guiot, J., Huntley, B., Jolly, D., Cheddadi, R., 1996. Reconstructing biomes from palaeoecological data: a general method and its application to European pollen data at 0 and 6 ka. Climate Dynamics 12, 185–194. https://doi.org/10.1007/BF00211617

Raberg, J.H., Flores, E., Crump, S.E., de Wet, G., Dildar, N., Miller, G.H., Geirsdóttir, Á., Sepúlveda, J., 2022. Intact Polar brGDGTs in Arctic Lake Catchments: Implications for Lipid Sources and Paleoclimate Applications. Journal of Geophysical Research: Biogeosciences 127, e2022JG006969. https://doi.org/10.1029/2022JG006969

Raberg, J.H., Harning, D.J., Crump, S.E., de Wet, G., Blumm, A., Kopf, S., Geirsdóttir, Á., Miller, G.H., Sepúlveda, J., 2021. Revised fractional abundances and warm-season temperatures substantially improve brGDGT calibrations in lake sediments. Biogeosciences 18, 3579–3603. https://doi.org/10.5194/bg-2021-16

Ramos-Román, M.J., De Jonge, C., Magyari, E., Veres, D., Ilvonen, L., Develle, A.-L., Seppä, H., 2022. Lipid biomarker (brGDGT)- and pollen-based reconstruction of temperature change during the Middle to Late Holocene transition in the Carpathians. Global and Planetary Change 215, 103859. https://doi.org/10.1016/j.gloplacha.2022.103859

Rasmussen, S.O., Bigler, M., Blockley, S.P., Blunier, T., Buchardt, S.L., Clausen, H.B., Cvijanovic, I., Dahl-Jensen, D., Johnsen, S.J., Fischer, H., Gkinis, V., Guillevic, M., Hoek, W.Z., Lowe, J.J., Pedro, J.B., Popp, T., Seierstad, I.K., Steffensen, J.P., Svensson, A.M., Vallelonga, P., Vinther, B.M., Walker, M.J.C., Wheatley, J.J., Winstrup, M., 2014. A stratigraphic framework for abrupt climatic changes during the Last Glacial period based on three synchronized Greenland ice-core records: refining and extending the INTIMATE event stratigraphy. Quaternary Science Reviews 106, 14–28. https://doi.org/10.1016/j.quascirev.2014.09.007

Rea, B.R., Pellitero, R., Spagnolo, M., Hughes, P., Ivy-Ochs, S., Renssen, H., Ribolini, A., Bakke, J., Lukas, S., Braithwaite, R.J., 2020. Atmospheric circulation over Europe during the Younger Dryas. Sci. Adv. 6, eaba4844. https://doi.org/10.1126/sciadv.aba4844

Regattieri, E., Zanchetta, G., Drysdale, R.N., Isola, I., Hellstrom, J.C., Dallai, L., 2014. Lateglacial to Holocene trace element record (Ba, Mg, Sr) from Corchia Cave (Apuan Alps, central Italy): paleoenvironmental implications: Trace element record from Corchia Cave, central Italy. J. Quaternary Sci. 29, 381–392. https://doi.org/10.1002/jqs.2712

Rehfeld, K., Münch, T., Ho, S.L., Laepple, T., 2018. Global patterns of declining temperature variability from the Last Glacial Maximum to the Holocene. Nature 554, 356–359. https://doi.org/10.1038/nature25454

Reille, M., 1998. Reille, Maurice, 1995. Pollen et spores d’Europe et d’Afrique du Nord, Supplément 1 . Éditions du Laboratoire de botanique historique et palynologie, Marseille, 327 p., 800 FF. / Reille, Maurice, 1998. Pollen et spores d’Europe et d’Afrique du Nord, Supplément 2 . Éditions du Laboratoire de botanique historique et palynologie, Marseille, 530 p., 1600 FF. gpq 52, 0–0. https://doi.org/10.7202/004885ar

Reimer, P.J., Austin, W.E.N., Bard, E., Bayliss, A., Blackwell, P.G., Ramsey, C.B., Butzin, M., Cheng, H., Edwards, R.L., Friedrich, M., Grootes, P.M., Guilderson, T.P., Hajdas, I., Heaton, T.J., Hogg, A.G., Hughen, K.A., Kromer, B., Manning, S.W., Muscheler, R., Palmer, J.G., Pearson, C., Plicht, J. van der, Reimer, R.W., Richards, D.A., Scott, E.M., Southon, J.R., Turney, C.S.M., Wacker, L., Adolphi, F., Büntgen, U., Capano, M., Fahrni, S.M., Fogtmann-Schulz, A., Friedrich, R., Köhler, P., Kudsk, S., Miyake, F., Olsen, J., Reinig, F., Sakamoto, M., Sookdeo, A., Talamo, S., 2020. The IntCal20 Northern Hemisphere Radiocarbon Age Calibration Curve (0–55 cal kBP). Radiocarbon 62, 725–757. https://doi.org/10.1017/RDC.2020.41

Renssen, H., Isarin, R.F.B., 2001. The two major warming phases of the last deglaciation at ∼14.7 and ∼11.5 ka cal BP in Europe: climate reconstructions and AGCM experiments. Global and Planetary Change 30, 117–153. https://doi.org/10.1016/S0921-8181(01)00082-0

Renssen, H., Mairesse, A., Goosse, H., Mathiot, P., Heiri, O., Roche, D.M., Nisancioglu, K.H., Valdes, P.J., 2015. Multiple causes of the Younger Dryas cold period. Nature Geosci 8, 946–949. https://doi.org/10.1038/ngeo2557

Robles, M., 2022. Vegetation, climate, and human history of the Mediterranean basin: A Late-Glacial to Holocene reconstruction from Italy (Lake Matese) to Armenia (Lake Sevan) inferred from a multi-proxy approach (pollen, NPPs, brGDGTs, XRF) (PhD thesis). University of Molise, University of Montpellier, Campobasso, Montpellier.

Robles, M., Peyron, O., Brugiapaglia, E., Ménot, G., Dugerdil, L., Ollivier, V., Ansanay-Alex, S., Develle, A.-L., Tozalakyan, P., Meliksetian, K., Sahakyan, K., Sahakyan, L., Perello, B., Badalyan, R., Colombié, C., Joannin, S., 2022. Impact of climate changes on vegetation and human societies during the Holocene in the South Caucasus (Vanevan, Armenia): A multiproxy approach including pollen, NPPs and brGDGTs. Quaternary Science Reviews 277, 107297. https://doi.org/10.1016/j.quascirev.2021.107297

Rodrigo-Gámiz, M., García-Alix, A., Jiménez-Moreno, G., Ramos-Román, M.J., Camuera, J., Toney, J.L., Sachse, D., Anderson, R.S., Sinninghe Damsté, J.S., 2022. Paleoclimate reconstruction of the last 36 kyr based on branched glycerol dialkyl glycerol tetraethers in the Padul palaeolake record (Sierra Nevada, southern Iberian Peninsula). Quaternary Science Reviews 281, 107434. https://doi.org/10.1016/j.quascirev.2022.107434

Russell, J.M., Hopmans, E.C., Loomis, S.E., Liang, J., Sinninghe Damsté, J.S., 2018. Distributions of 5- and 6-methyl branched glycerol dialkyl glycerol tetraethers (brGDGTs) in East African lake sediment: Effects of temperature, pH, and new lacustrine paleotemperature calibrations. Organic Geochemistry 117, 56–69. https://doi.org/10.1016/j.orggeochem.2017.12.003

Sadori, L., 2018. The Lateglacial and Holocene vegetation and climate history of Lago di Mezzano (central Italy). Quaternary Science Reviews 202, 30–44. https://doi.org/10.1016/j.quascirev.2018.09.004

Salonen, J.S., Korpela, M., Williams, J.W., Luoto, M., 2019. Machine-learning based reconstructions of primary and secondary climate variables from North American and European fossil pollen data. Sci Rep 9, 15805. https://doi.org/10.1038/s41598-019-52293-4

Samartin, S., Heiri, O., Joos, F., Renssen, H., Franke, J., Brönnimann, S., Tinner, W., 2017. Warm Mediterranean mid-Holocene summers inferred from fossil midge assemblages. Nature Geosci 10, 207–212. https://doi.org/10.1038/ngeo2891

Sanchi, L., Ménot, G., Bard, E., 2014. Insights into continental temperatures in the northwestern Black Sea area during the Last Glacial period using branched tetraether lipids. Quaternary Science Reviews 84, 98–108. https://doi.org/10.1016/j.quascirev.2013.11.013

Sbaffi, L., Wezel, F.C., Curzi, G., Zoppi, U., 2004. Millennial- to centennial-scale palaeoclimatic variations during Termination I and the Holocene in the central Mediterranean Sea. Global and Planetary Change 40, 201–217. https://doi.org/10.1016/S0921-8181(03)00111-5

Sicre, M.-A., Siani, G., Genty, D., Kallel, N., Essallami, L., 2013. Seemingly divergent sea surface temperature proxy records in the central Mediterranean during the last deglacial. Climate of the Past 9, 1375–1383. https://doi.org/10.5194/cpd-9-683-2013

Sinninghe Damsté, J.S., Rijpstra, W.I.C., Foesel, B.U., Huber, K.J., Overmann, J., Nakagawa, S., Kim, J.J., Dunfield, P.F., Dedysh, S.N., Villanueva, L., 2018. An overview of the occurrence of ether- and ester-linked iso-diabolic acid membrane lipids in microbial cultures of the Acidobacteria: Implications for brGDGT paleoproxies for temperature and pH. Organic Geochemistry 124, 63–76. https://doi.org/10.1016/j.orggeochem.2018.07.006

Smith, V.C., Isaia, R., Pearce, N.J.G., 2011. Tephrostratigraphy and glass compositions of post-15 kyr Campi Flegrei eruptions: implications for eruption history and chronostratigraphic markers. Quaternary Science Reviews 30, 3638–3660. https://doi.org/10.1016/j.quascirev.2011.07.012

Stockhecke, M., Bechtel, A., Peterse, F., Guillemot, T., Schubert, C.J., 2021. Temperature, precipitation, and vegetation changes in the Eastern Mediterranean over the last deglaciation and Dansgaard-Oeschger events. Palaeogeography, Palaeoclimatology, Palaeoecology 577, 110535. https://doi.org/10.1016/j.palaeo.2021.110535

Sun, Q., Chu, G., Liu, M., Xie, M., Li, S., Ling, Y., Wang, X., Shi, L., Jia, G., Lü, H., 2011. Distributions and temperature dependence of branched glycerol dialkyl glycerol tetraethers in recent lacustrine sediments from China and Nepal. J. Geophys. Res. 116, G01008. https://doi.org/10.1029/2010JG001365

Taffetani, F., Catorci, A., Ciaschetti, G., Cutini, M., Di Martino, L., Frattaroli, A.R., Paura, B., Pirone, G., Rismondo, M., Zitti, S., 2012. The Quercus cerris woods of the alliance Carpinion orientalis Horvat 1958 in Italy. Plant Biosystems - An International Journal Dealing with all Aspects of Plant Biology 146, 918–953. https://doi.org/10.1080/11263504.2012.682613

Tarroso, P., Carrión, J., Dorado-Valiño, M., Queiroz, P., Santos, L., Valdeolmillos-Rodríguez, A., Célio Alves, P., Brito, J.C., Cheddadi, R., 2016. Spatial climate dynamics in the Iberian Peninsula since 15 000 yr BP. Climate of the Past 12, 1137–1149. https://doi.org/10.5194/cp-12-1137-2016

ter Braak, C.J.F., Juggins, S., 1993. Weighted averaging partial least squares regression (WA-PLS): an improved method for reconstructing environmental variables from species assemblages 18.

ter Braak, C.J.F., van Dam, H., 1989. Inferring pH from diatoms: a comparison of old and new calibration methods. Hydrobiologia 178, 209–223. https://doi.org/10.1007/BF00006028

Tomlinson, E.L., Arienzo, I., Civetta, L., Wulf, S., Smith, V.C., Hardiman, M., Lane, C.S., Carandente, A., Orsi, G., Rosi, M., Müller, W., Menzies, M.A., 2012. Geochemistry of the Phlegraean Fields (Italy) proximal sources for major Mediterranean tephras:

Implications for the dispersal of Plinian and co-ignimbritic components of explosive eruptions. Geochimica et Cosmochimica Acta 93, 102–128. https://doi.org/10.1016/j.gca.2012.05.043

Valente, E., Buscher, J.T., Jourdan, F., Petrosino, P., Reddy, S.M., Tavani, S., Corradetti, A., Ascione, A., 2019. Constraining mountain front tectonic activity in extensional setting from geomorphology and Quaternary stratigraphy: A case study from the Matese ridge, southern Apennines. Quaternary Science Reviews 219, 47–67. https://doi.org/10.1016/j.quascirev.2019.07.001

Van Geel, B., 2002. Non-Pollen Palynomorphs, in: Smol, J.P., Birks, H.J.B., Last, W.M., Bradley, R.S., Alverson, K. (Eds.), Tracking Environmental Change Using Lake Sediments, Developments in Paleoenvironmental Research. Springer Netherlands, Dordrecht, pp. 99–119. https://doi.org/10.1007/0-306-47668-1_6

Vescovi, E., Kaltenrieder, P., Tinner, W., 2010. Late-Glacial and Holocene vegetation history of Pavullo nel Frignano (Northern Apennines, Italy). Review of Palaeobotany and Palynology 160, 32–45. https://doi.org/10.1016/j.revpalbo.2010.01.002

Walker, M., Lowe, J., Blockley, S.P.E., Bryant, C., Coombes, P., Davies, S., Hardiman, M., Turney, C.S.M., Watson, J., 2012. Lateglacial and early Holocene palaeoenvironmental ‘events’ in Sluggan Bog, Northern Ireland: comparisons with the Greenland NGRIP GICC05 event stratigraphy. Quaternary Science Reviews 36, 124–138. https://doi.org/10.1016/j.quascirev.2011.09.008

Watson, B.I., Williams, J.W., Russell, J.M., Jackson, S.T., Shane, L., Lowell, T.V., 2018. Temperature variations in the southern Great Lakes during the last deglaciation: Comparison between pollen and GDGT proxies. Quaternary Science Reviews 182, 78–92. https://doi.org/10.1016/j.quascirev.2017.12.011

Weijers, J.W.H., Panoto, E., van Bleijswijk, J., Schouten, S., Rijpstra, W.I.C., Balk, M., Stams, A.J.M., Damsté, J.S.S., 2009. Constraints on the Biological Source(s) of the Orphan Branched Tetraether Membrane Lipids. Geomicrobiology Journal 26, 402–414. https://doi.org/10.1080/01490450902937293

Weijers, J.W.H., Schouten, S., Spaargaren, O.C., Sinninghe Damsté, J.S., 2006. Occurrence and distribution of tetraether membrane lipids in soils: Implications for the use of the TEX86 proxy and the BIT index. Organic Geochemistry 37, 1680–1693. https://doi.org/10.1016/j.orggeochem.2006.07.018

Weijers, J.W.H., Schouten, S., van den Donker, J.C., Hopmans, E.C., Sinninghe Damsté, J.S., 2007. Environmental controls on bacterial tetraether membrane lipid distribution in soils. Geochimica et Cosmochimica Acta 71, 703–713. https://doi.org/10.1016/j.gca.2006.10.003

Wulf, S., Kraml, M., Brauer, A., Keller, J., Negendank, J.F.W., 2004. Tephrochronology of the 100ka lacustrine sediment record of Lago Grande di Monticchio (southern Italy). Quaternary International 122, 7–30. https://doi.org/10.1016/j.quaint.2004.01.028

Wulf, S., Kraml, M., Keller, J., 2008. Towards a detailed distal tephrostratigraphy in the Central Mediterranean: The last 20,000 yrs record of Lago Grande di Monticchio. Journal of Volcanology and Geothermal Research 177, 118–132. https://doi.org/10.1016/j.jvolgeores.2007.10.009

Yang, H., Pancost, R.D., Dang, X., Zhou, X., Evershed, R.P., Xiao, G., Tang, C., Gao, L., Guo, Z., Xie, S., 2014. Correlations between microbial tetraether lipids and environmental variables in Chinese soils: Optimizing the paleo-reconstructions in semi-arid and arid regions. Geochimica et Cosmochimica Acta 126, 49–69. https://doi.org/10.1016/j.gca.2013.10.041

Zhang, J., Bai, Y., Xu, S., Lei, F., Jia, G., 2013. Alkenone and tetraether lipids reflect different seasonal seawater temperatures in the coastal northern South China Sea. Organic Geochemistry 58, 115–120. https://doi.org/10.1016/j.orggeochem.2013.02.012